7 LDA+DMFT: Multi-Orbital Hubbard Models

Eva Pavarini
Institute for Advanced Simulation
Forschungszentrum Jülich

Contents

E. Pavarini, E. Koch, A. Lichtenstein, and D. Vollhardt (eds.)
DMFT: From Infinite Dimensions to Real Materials
Modeling and Simulation Vol. 8
Forschungszentrum Jülich, 2018, ISBN 978-3-95806-313-6
http://www.cond-mat.de/events/correl18

1 Introduction

Most electronic properties of solids and molecules can be described – in the non-relativistic limit and in the Born-Oppenheimer approximation – by the electronic many-body Hamiltonian

$$\hat{H}_e^{\rm NR} = -\frac{1}{2}\sum_i \nabla_i^2 - \sum_i \sum_\alpha \frac{Z_\alpha}{|\boldsymbol{r}_i - \boldsymbol{R}_\alpha|} + \sum_{i>j} \frac{1}{|\boldsymbol{r}_i - \boldsymbol{r}_j|} + \sum_{\alpha>\alpha'} \frac{Z_\alpha Z_{\alpha'}}{|\boldsymbol{R}_\alpha - \boldsymbol{R}_{\alpha'}|} \qquad (1)$$

In practice, finding the exact eigenvalues and eigenvector of this Hamiltonian for a given system is impossible, unless the number of electrons is very small. This might sound as a gloomy conclusion for condensed-matter physics. The positive side is that, however, the exact solution of the many-body Hamiltonian (1) is, most likely, not even useful for understanding the properties of matter. One can grasp the reason by looking to a many-body problem for which an exact solution was found, the classical gravitational N-body system. Even without the complication of quantum mechanics, describing the behavior of many *interacting* classical bodies is a formidable task. This complexity is remarkable, since in the absence of interactions everything seems beautifully simple. Let us remind ourselves why. If a system is made of a single body with mass m_1, and its initial position, $\boldsymbol{r}_1(0)$, and velocity, $\dot{\boldsymbol{r}}_1(0)$, are known, we can predict its position at any time in the future by solving the trivial equation

$$m_1 \ddot{\boldsymbol{r}}_1 = 0.$$

If our system contains two such bodies, we can just do the same, the only possible complication being collisions; as a matter of fact, if we exclude collisions, the first body does not influence at all the second. The system of independent equations that we have to solve is just

$$m_1 \ddot{\boldsymbol{r}}_1 \;\; = 0 \;\; \wedge \;\; m_2 \ddot{\boldsymbol{r}}_2 \;\; = 0.$$

In the large-N limit, assuming that all bodies have the same mass $m_i = m$ and collisions are elastic, the system behaves as an ideal gas, whose macroscopic properties are described by the famous ideal-gas law $PV = Nk_BT$. As soon as we switch on the gravitational interaction, however, everything is suddenly awfully complicated. The two-body problem is already difficult by itself. The system of equations is now

$$\begin{cases} m_1 \ddot{\boldsymbol{r}}_1 \;\; = +\boldsymbol{F}_{12} \\ m_2 \ddot{\boldsymbol{r}}_2 \;\; = -\boldsymbol{F}_{12} \end{cases}$$

where

$$\boldsymbol{F}_{12} = -\frac{G m_1 m_2 \hat{\boldsymbol{r}}}{r^2}, \qquad \boldsymbol{r} = \boldsymbol{r}_1 - \boldsymbol{r}_2$$

is the force that the second body exerts on the first. This system can be solved exactly after changing variables to the center-of-mass and relative coordinates. Its solution yields a surprising emerging behavior, i.e., closed elliptical orbits. Let us add now one body more

$$\begin{cases} m_1 \ddot{\boldsymbol{r}}_1 \;\; = +\boldsymbol{F}_{12} + \boldsymbol{F}_{13} \\ m_2 \ddot{\boldsymbol{r}}_2 \;\; = -\boldsymbol{F}_{12} + \boldsymbol{F}_{23} \\ m_3 \ddot{\boldsymbol{r}}_3 \;\; = -\boldsymbol{F}_{13} - \boldsymbol{F}_{23}. \end{cases} \qquad (2)$$

The three-body problem (2) was a mystery for a long time. It can even present *chaotic effects*; when chaos reigns, the behavior of the system in the future is very sensitive to small changes in the initial conditions. The problem was solved by Karl F. Sundman at the beginning of last century, who found – few cases excluded – a convergent series solution in powers of $t^{1/3}$ [1]. The extension to the general N-body problem arrived in 1991 thanks to Qiudong Wang, at the time a young researcher. This story is nicely told in a review article by Florin Diacu [2], who concludes

> *Did this mean the end of the N-body problem? Was this old question – unsuccessfully attacked by the greatest mathematicians of the last three centuries – merely solved by a student in a moment of rare inspiration? [..] Paradoxically [..] not; in fact we know nothing more than before having that solution.*

The explanation is that

> *[..] these series solutions [...] have very slow convergence. One would have to sum up millions of terms to determine the motions of the particles for insignificantly short intervals of time. The round-off errors make these series unusable in numerical works. From the theoretical point of view, these solution add nothing to what was previously known about the N-body problem.*

Indeed, we are not even interested in knowing where all particles are at each moment. We do not want to reproduce the complete history of the formation of the solar system, atom by atom. We rather look for answers to questions such as "Is the solar system stable? If not, in what time frame will chaotic behavior manifest itself?". We can now foresee that a similar conclusion would likely apply to the quantum case, had we at hand the exact solution of this, even more complex, N-body problem. Such a solution would contain too much information. We would need the lifetime of the universe or longer for extracting the answer to one of our questions, e.g., "why are some systems metals and other insulators?" or " what is the origin of superconductivity?". We would *perfectly reproduce experimental phenomena*, without being able to tell anything about their origin.[1] We have thus to abandon the idea that all problems can be solved by a single magic algorithm which returns the exact solution, unless we can, in addition, build an oracle machine powerful enough to eliminate all the irrelevant data and identify the essential elements, providing answers to the real questions. We cannot exclude that one day artificial intelligence will be able to do that for us [3]. In the mean time, the strategy is to build minimal materials-specific models which capture the essence of the phenomenon we want to understand, and solve them as accurately as possible. Unfortunately, even for those models, in most cases only approximate solutions are available. Thus the simplifications made and the approximations adopted have to be put to the test. In this imperfect world, in which neither the model nor the solution method are exact, and in which there is no guarantee that the choices we made are indeed good enough, we have to try to explain reality. Finding realistic

[1] Indeed, agreement with experiments is highly overrated. A useful theory should explain, not merely reproduce, experimental measurements.

but minimal models (and, at the same time approximate methods of solution that work) is, of course, not at all trivial, and often involves refinements and corrections. This approach, despite its non-systematic, trial-and-error nature, proved itself very successful and allowed physicists to understand superconductivity, the Kondo effect, the metal-insulator transition, and much more. The first step to make progress is to rewrite the Hamiltonian in second quantization, the formalism that allows us to deal with many-body states and operators in a compact and elegant way. It is worth to remind ourselves that setting up the Hamiltonian in second quantization requires to identify and choose a complete *one-electron basis*. The selection of the basis is important, because certain choices allow us to build *better* models than others. Here *better* indicates a more advantageous compromise between two competing needs, *(i)* that the model is as realistic as possible and *(ii)* that its associated Fock space is as small as possible. The role of the basis becomes perhaps more clear with a simple example. The low-energy bound states of the hydrogen atom can be described, of course, in a basis of plane waves; the number of plane waves required is extremely high, however. In the many-body case, the basis might make the difference between being able to solve the relevant model or not. In this lecture we will adopt as basis Wannier functions, $\psi_{im\sigma}(\boldsymbol{r})$. First we will write the Hamiltonian using the complete set, and later we will see how to construct minimal models. Using a complete set of Wannier functions, the Hamiltonian (1) can be expressed as $\hat{H}_e = \hat{H}_0 + \hat{H}_U$. The one-electron term, $\hat{H}_0$, describes the kinetic energy and the attraction between electrons and nuclei, and is given by

$$\hat{H}_0 = -\sum_{\sigma}\sum_{ii'}\sum_{mm'} t^{i,i'}_{m,m'}\, c^{\dagger}_{im\sigma} c_{i'm'\sigma}.$$

Here $c^{\dagger}_{im\sigma}$ ($c_{im\sigma}$) creates (destroys) an electron with spin σ in orbital m at site i. The on-site ($i = i'$) terms yield the crystal-field matrix $\varepsilon_{m,m'} = t^{i,i}_{m,m'}$ while the $i \neq i'$ contributions are the hopping integrals. The parameters are given by

$$t^{i,i'}_{m,m'} = -\int d\mathbf{r}\, \overline{\psi_{im\sigma}}(\boldsymbol{r})\Big(-\frac{1}{2}\nabla^2 + v_{\rm R}(\boldsymbol{r})\Big)\psi_{i'm'\sigma}(\boldsymbol{r}), \tag{3}$$

where $v_R(\boldsymbol{r})$ is the electron-nuclei interaction. The electron-electron repulsion $\hat{H}_U$ is

$$\hat{H}_U = \frac{1}{2}\sum_{ii'jj'}\sum_{\sigma\sigma'}\sum_{mm'pp'} U^{iji'j'}_{mp\,m'p'}\, c^{\dagger}_{im\sigma} c^{\dagger}_{jp\sigma'} c_{j'p'\sigma'} c_{i'm'\sigma},$$

where the (*bare*) Coulomb integrals can be expressed as

$$U^{iji'j'}_{mp\,m'p'} = \int d\boldsymbol{r}_1 \int d\boldsymbol{r}_2\, \overline{\psi_{im\sigma}}(\boldsymbol{r}_1)\overline{\psi_{jp\sigma'}}(\boldsymbol{r}_2)\frac{1}{|\boldsymbol{r}_1 - \boldsymbol{r}_2|}\psi_{j'p'\sigma'}(\boldsymbol{r}_2)\psi_{i'm'\sigma}(\boldsymbol{r}_1).$$

The simplest version of $\hat{H}_e$ is the so-called Hubbard model, in which we consider only one orbital ($m{=}m'{=}p{=}p'$) and we assume that the Coulomb term is local ($i{=}i'{=}j{=}j'$). This yields

$$\hat{H} = -\sum_{\sigma}\sum_{ii'} t^{i,i'} c^{\dagger}_{i\sigma} c_{i'\sigma} + U\sum_i \hat{n}_{i\uparrow}\hat{n}_{i\downarrow} = \sum_{\boldsymbol{k}\sigma} \varepsilon_{\boldsymbol{k}} c^{\dagger}_{\boldsymbol{k}\sigma} c_{\boldsymbol{k}\sigma} + U\sum_i \hat{n}_{i\uparrow}\hat{n}_{i\downarrow}. \tag{4}$$

Even this apparently simple model cannot be solved exactly in the general case. This is because it contains already all the essence of the electronic many-body problem.

2 LDA+DMFT

The Hubbard model (4) and its multi-orbital generalizations are the minimal models for describing the Mott metal-insulator transition. The most successful method of solution capturing the nature of the Mott transition is DMFT, dynamical mean-field theory [4–7]. It is based on the local self-energy approximation, i.e., the assumption that $\Sigma^\sigma(\boldsymbol{k},\omega) \sim \Sigma^\sigma_l(\omega)$. DMFT is exact for $U = 0$ (band limit), for $t^{i,i'} = 0$ (atomic limit), and in the limit of infinite coordination number [4, 5]. In the present section we will illustrate the basic ideas of this approach. First we will use a toy model that can be solved analytically, the Hubbard dimer. For this model the coordination number is equal to one, and thus, as one might expect, a local self-energy is a bad approximation. The example is nevertheless very useful to explain the essence of the method. Next we will extend to the one-band Hubbard model, and finally we will generalize to realistic multi-orbital many-body Hamiltonians.

2.1 DMFT for the Hubbard dimer

The two-site Hubbard model is given by

$$\hat{H} = \varepsilon_d \sum_{i\sigma} \hat{n}_{i\sigma} - t \sum_{\sigma} \left(c^\dagger_{1\sigma} c_{2\sigma} + c^\dagger_{2\sigma} c_{1\sigma} \right) + U \sum_i \hat{n}_{i\uparrow} \hat{n}_{i\downarrow},$$

with $i = 1, 2$. The ground-state for $N = 2$ electrons (half filling) is the singlet[2]

$$|G\rangle_H = |2, 00\rangle_- = \frac{a_2}{\sqrt{2}} \left[c^\dagger_{1\uparrow} c^\dagger_{2\downarrow} - c^\dagger_{1\downarrow} c^\dagger_{2\uparrow} \right] |0\rangle + \frac{a_1}{\sqrt{2}} \left[c^\dagger_{1\uparrow} c^\dagger_{1\downarrow} + c^\dagger_{2\uparrow} c^\dagger_{2\downarrow} \right] |0\rangle \tag{5}$$

with

$$a_1^2 = \frac{1}{\Delta(t,U)} \frac{\Delta(t,U) - U}{2}, \qquad a_2^2 = \frac{4t^2}{\Delta(t,U)} \frac{2}{\Delta(t,U) - U},$$

and

$$\Delta(t,U) = \sqrt{U^2 + 16t^2}.$$

The energy of this state is

$$E_0(2) = 2\varepsilon_d + \frac{1}{2}\big(U - \Delta(t,U)\big).$$

In the $T \to 0$ limit, the exact local Matsubara Green function for spin σ takes then the form

$$G^\sigma_{i,i}(i\nu_n) = \frac{1}{4} \left[\frac{1+w}{i\nu_n - (E_0(2) - \varepsilon_d + t - \mu)} + \frac{1-w}{i\nu_n - (E_0(2) - \varepsilon_d - t - \mu)} \right.$$
$$\left. + \frac{1-w}{i\nu_n - (-E_0(2) + U + 3\varepsilon_d + t - \mu)} + \frac{1+w}{i\nu_n - (-E_0(2) + U + 3\varepsilon_d - t - \mu)} \right],$$

[2] You can find all eigenstates and eigenvalues of this model for arbitrary filling in my chapter in Ref. [8].

where $\nu_n = \pi(2n+1)/\beta$ are fermionic Matsubara frequencies, $\mu = \varepsilon_d + U/2$ is the chemical potential, and the weight is $w = 2a_1a_2$. The local Green function can be rewritten as the average of the Green function for the bonding ($k = 0$) and the anti-bonding state ($k = \pi$), i.e.,

$$G^\sigma_{i,i}(i\nu_n) = \frac{1}{2}\Bigg(\underbrace{\frac{1}{i\nu_n + \mu - \varepsilon_d + t - \Sigma^\sigma(0, i\nu_n)}}_{G^\sigma(0,i\nu_n)} + \underbrace{\frac{1}{i\nu_n + \mu - \varepsilon_d - t - \Sigma^\sigma(\pi, i\nu_n)}}_{G^\sigma(\pi,i\nu_n)} \Bigg).$$

The self-energy is given by

$$\Sigma^\sigma(k, i\nu_n) = \frac{U}{2} + \frac{U^2}{4}\frac{1}{i\nu_n - \ e^{ik}\ 3t}.$$

The self-energies $\Sigma^\sigma(0, i\nu_n)$ and $\Sigma^\sigma(\pi, i\nu_n)$ differ due to the phase $e^{ik} = \pm 1$ in their denominators. The local self-energy is, by definition, the average of the two

$$\Sigma^\sigma_l(i\nu_n) = \frac{1}{2}\Big(\Sigma^\sigma(\pi, i\nu_n) + \Sigma^\sigma(0, i\nu_n) \Big) = \frac{U}{2} + \frac{U^2}{4}\ \frac{i\nu_n}{(i\nu_n)^2 - (3t)^2}.$$

The difference

$$\Delta\Sigma^\sigma_l(i\nu_n) = \frac{1}{2}\Big(\Sigma^\sigma(\pi, i\nu_n) - \Sigma^\sigma(0, i\nu_n) \Big),$$

thus measures the importance of non-local effects; it would be zero if the self-energy was independent of $\boldsymbol{k}$. Next we define the hybridization function

$$F^\sigma(i\nu_n) = \frac{\big(t + \Delta\Sigma^\sigma_l(i\nu_n)\big)^2}{i\nu_n + \mu - \varepsilon_d - \Sigma^\sigma_l(i\nu_n)}$$

which for $U = 0$ becomes

$$F^\sigma_0(i\nu_n) = \frac{t^2}{i\nu_n}.$$

By using these definitions, we can rewrite the local Green function as

$$G^\sigma_{i,i}(i\nu_n) = \frac{1}{i\nu_n + \mu - \varepsilon_d - F^\sigma(i\nu_n) - \Sigma^\sigma_l(i\nu_n)}.$$

It is important to point out that the local Green function and the local self-energy satisfy the following *local Dyson equation*

$$\Sigma^\sigma_l(i\nu_n) = \frac{1}{\mathfrak{G}^\sigma_{i,i}(i\nu_n)} - \frac{1}{G^\sigma_{i,i}(i\nu_n)},$$

where $\mathfrak{G}^\sigma_{i,i}(i\nu_n)$ is given by

$$\mathfrak{G}^\sigma_{i,i}(i\nu_n) = \frac{1}{i\nu_n + \mu - \varepsilon_d - F^\sigma(i\nu_n)}.$$

Thus, one could think of mapping the Hubbard dimer into an auxiliary quantum-impurity model, chosen such that, within certain approximations, the impurity Green function is close to the local Green function of the original problem. Is this possible? Let us adopt as auxiliary model the Anderson molecule

$$\hat{H}^{\mathrm{A}} = \varepsilon_s \sum_\sigma \hat{n}_{s\sigma} - t \sum_\sigma \left(c^\dagger_{d\sigma} c_{s\sigma} + c^\dagger_{s\sigma} c_{d\sigma} \right) + \varepsilon_d \sum_\sigma \hat{n}_{d\sigma} + U \hat{n}_{d\uparrow} \hat{n}_{d\downarrow}. \tag{6}$$

The first constraint would be that Hamiltonian (6) has a ground state with the same occupations of the 2-site Hubbard model, i.e., at half filling, $n_d = n_s = 1$. The condition is satisfied if $\varepsilon_s = \mu$. This can be understood by comparing the Hamiltonian matrices of the two models in the Hilbert space with $N = 2$ electrons. Let us order the two-electron states of the Hubbard dimer as

$$\begin{aligned}
|1\rangle = \ & |2,1,1\rangle & = \ & c^\dagger_{1\uparrow} c^\dagger_{2\uparrow} |0\rangle, \\
|2\rangle = \ & |2,1,-1\rangle & = \ & c^\dagger_{1\downarrow} c^\dagger_{2\downarrow} |0\rangle, \\
|3\rangle = \ & |2,1,0\rangle & = \ & \tfrac{1}{\sqrt{2}} [c^\dagger_{1\uparrow} c^\dagger_{2\downarrow} + c^\dagger_{1\downarrow} c^\dagger_{2\uparrow}] |0\rangle, \\
|4\rangle = \ & |2,0,0\rangle & = \ & \tfrac{1}{\sqrt{2}} [c^\dagger_{1\uparrow} c^\dagger_{2\downarrow} - c^\dagger_{1\downarrow} c^\dagger_{2\uparrow}] |0\rangle, \\
|5\rangle = \ & |2,0,0\rangle_1 & = \ & c^\dagger_{1\uparrow} c^\dagger_{1\downarrow} |0\rangle, \\
|6\rangle = \ & |2,0,0\rangle_2 & = \ & c^\dagger_{2\uparrow} c^\dagger_{2\downarrow} |0\rangle.
\end{aligned}$$

In this basis the Hamiltonian has the matrix form

$$\hat{H}_2 = \begin{pmatrix}
2\varepsilon_d & 0 & 0 & 0 & 0 & 0 \\
0 & 2\varepsilon_d & 0 & 0 & 0 & 0 \\
0 & 0 & 2\varepsilon_d & 0 & 0 & 0 \\
0 & 0 & 0 & 2\varepsilon_d & -\sqrt{2}t & -\sqrt{2}t \\
0 & 0 & 0 & -\sqrt{2}t & 2\varepsilon_d{+}U & 0 \\
0 & 0 & 0 & -\sqrt{2}t & 0 & 2\varepsilon_d{+}U
\end{pmatrix}.$$

The ground state, the singlet given in Eq. (5), can be obtained by diagonalizing the lower $3{\times}3$ block. For the Anderson molecule, ordering the basis in the same way ($1 \to d, 2 \to s$), this Hamiltonian becomes

$$\hat{H}_2^A = \begin{pmatrix}
\varepsilon_d{+}\varepsilon_s & 0 & 0 & 0 & 0 & 0 \\
0 & \varepsilon_d{+}\varepsilon_s & 0 & 0 & 0 & 0 \\
0 & 0 & \varepsilon_d{+}\varepsilon_s & 0 & 0 & 0 \\
0 & 0 & 0 & \varepsilon_d{+}\varepsilon_s & -\sqrt{2}t & -\sqrt{2}t \\
0 & 0 & 0 & -\sqrt{2}t & 2\varepsilon_d{+}U & 0 \\
0 & 0 & 0 & -\sqrt{2}t & 0 & 2\varepsilon_s
\end{pmatrix}.$$

By comparison, we may see that if $\varepsilon_s = \varepsilon_d + U/2$, the ground-state of $\hat{H}_2^A$ has the form of the ground-state for the Hubbard dimer, i.e.,

$$|G\rangle_A = \frac{\alpha_2}{\sqrt{2}}\left[c^\dagger_{d\uparrow}c^\dagger_{s\downarrow} - c^\dagger_{d\downarrow}c^\dagger_{s\uparrow}\right]|0\rangle + \frac{\alpha_1}{\sqrt{2}}\left[c^\dagger_{d\uparrow}c^\dagger_{d\downarrow} + c^\dagger_{s\uparrow}c^\dagger_{s\downarrow}\right]|0\rangle.$$

The values of α_1 and α_2, as well as the complete list of eigenvalues and eigenvectors of the Anderson molecule for $\varepsilon_s = \varepsilon_d + U/2$ and arbitrary electron number N, can be found in the Appendix. The impurity Green function takes then the form

$$G^\sigma_{d,d}(i\nu_n) = \frac{1}{4}\Bigg[\frac{1+w'}{i\nu_n - (E_0(2) - E_-(1) - \mu)} + \frac{1-w'}{i\nu_n - (E_0(2) - E_+(1) - \mu)} \\ \frac{1+w'}{i\nu_n - (E_-(3) - E_0(2) - \mu)} + \frac{1-w'}{i\nu_n - (E_+(3) - E_0(2) - \mu)}\Bigg],$$

where

$$E_0(2) - E_\pm(1) - \mu = -\frac{1}{4}\Big(2\Delta(t,U/2) \pm \Delta(t,U)\Big),$$

$$E_\pm(3) - E_0(2) - \mu = +\frac{1}{4}\Big(2\Delta(t,U/2) \pm \Delta(t,U)\Big),$$

$$w' = \frac{1}{2}\frac{32t^2 - U^2}{\Delta(t,U)\Delta(t,U/2)}.$$

After some rearrangement we obtain a much simpler expression

$$G^\sigma_{d,d}(i\nu_n) = \frac{1}{i\nu_n + \mu - \varepsilon_d - \mathcal{F}^\sigma_0(i\nu_n) - \Sigma^\sigma_A(i\nu_n)}.$$

The impurity self-energy equals the local self-energy of the Hubbard dimer

$$\Sigma^\sigma_A(i\nu_n) = \frac{U}{2} + \frac{U^2}{4}\frac{i\nu_n}{(i\nu_n)^2 - (3t)^2}.$$

The hybridization function is given by

$$\mathcal{F}^\sigma_0(i\nu_n) = \frac{t^2}{i\nu_n}.$$

For $U = 0$, $G^\sigma_{d,d}(i\nu_n)$ equals the non-interacting impurity Green function

$$G^{0\sigma}_{d,d}(i\nu_n) = \frac{1}{i\nu_n + \mu - \varepsilon_d - \mathcal{F}^\sigma_0(i\nu_n)}.$$

The impurity Green function thus satisfies the *impurity Dyson equation*

$$\Sigma^\sigma_A(i\nu_n) = \frac{1}{G^{0\sigma}_{d,d}(i\nu_n)} - \frac{1}{G^\sigma_{d,d}(i\nu_n)}.$$

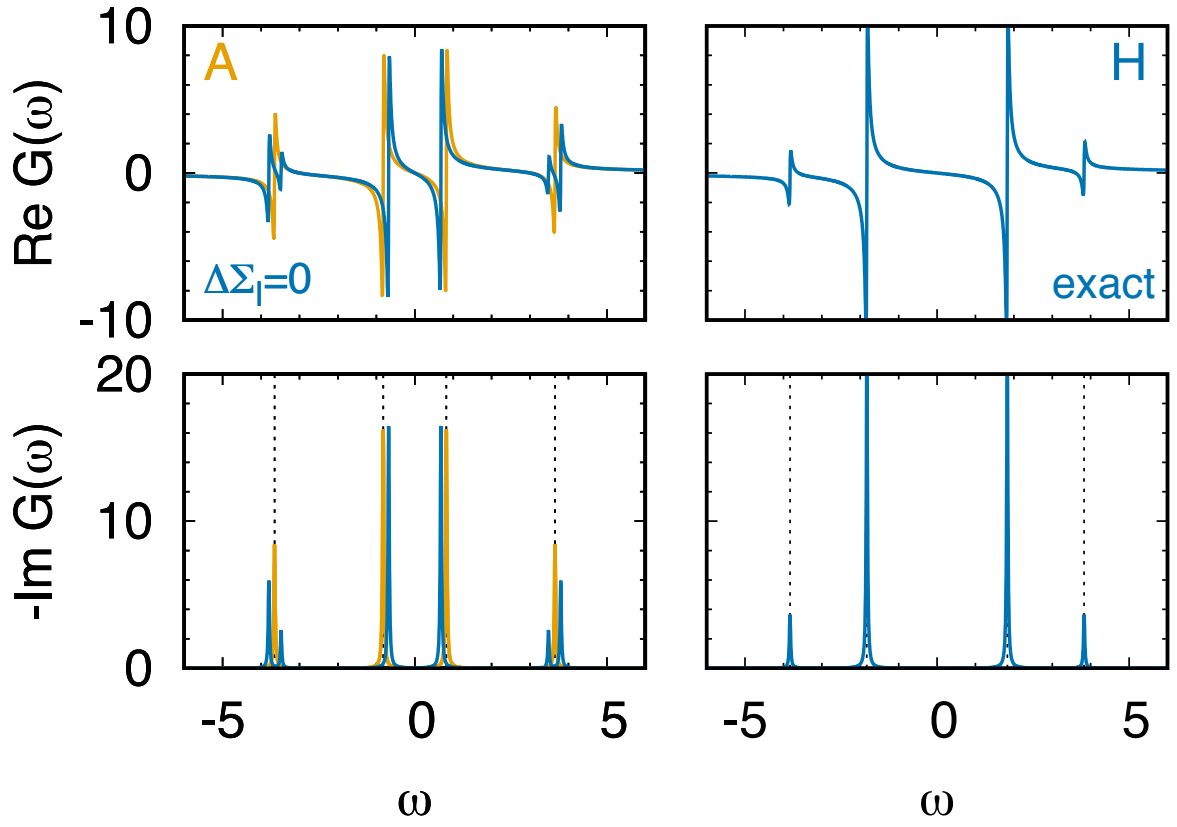

Fig. 1: *Green functions of the Hubbard dimer ($t = 1, U = 4$) and the Anderson molecule ($\varepsilon_s = \varepsilon_d + U/2$) in the zero temperature limit. Left panels, blue: Hubbard dimer with local self-energy only, i.e., with $\Delta\Sigma_l^\sigma(\omega) = 0$. Left panels, orange: Anderson molecule. Right panels: Exact Green function of the Hubbard dimer. Dashed lines: poles of the Green function of the Anderson molecule (left) or Hubbard dimer (right).*

In Fig. 1 we show the impurity Green function of the Anderson molecule (orange, left panels) and the local Green function of the 2-site Hubbard model, in the local self-energy approximation (blue, left panels) and exact (blue, right panels). Comparing left and right panels we can see that setting $\Delta\Sigma_l^\sigma(\omega) = 0$ yields large errors. The left panels demonstrate, however, that the spectral function of the Anderson molecule is quite similar to the one of the Hubbard dimer with $\Delta\Sigma_l^\sigma(\omega) = 0$. The small remaining deviations come from replacing, in the impurity Dyson equation, the non-interacting impurity Green function with $\mathfrak{G}_{i,i}^\sigma(i\nu_n)$ in the local self-energy approximation, i.e., with the *bath* Green function

$$\mathcal{G}_{i,i}^\sigma(i\nu_n) = \frac{1}{i\nu_n + \mu - \varepsilon_d - \mathcal{F}_l^\sigma(i\nu_n)},$$

where

$$\mathcal{F}_l^\sigma(i\nu_n) = \frac{t^2}{i\nu_n + \mu - \varepsilon_d - \Sigma_A^\sigma(i\nu_n)}.$$

We are now in the position of explaining how DMFT works for the Hamiltonian of the Hubbard dimer, choosing the Anderson molecule Hamiltonian (6) as the auxiliary quantum-impurity model. The procedure can be split in the following steps

1. Build the initial quantum impurity model with $G^{0\sigma}_{d,d}(i\nu_n) = G^{0\sigma}_{i,i}(i\nu_n)$. The initial bath is thus defined by energy $\varepsilon_s = \varepsilon_d$ and hopping t.

2. Calculate the local Green function $G^{\sigma}_{d,d}(i\nu_n)$ for the auxiliary model.

3. Use the local Dyson equation to calculate the impurity self-energy

$$\Sigma^{\sigma}_A(i\nu_n) = \frac{1}{G^{0\sigma}_{d,d}(i\nu_n)} - \frac{1}{G^{\sigma}_{d,d}(i\nu_n)}.$$

4. Calculate the local Green function of the Hubbard dimer setting the self-energy equal to the one of the quantum-impurity model

$$G^{\sigma}_{i,i}(i\nu_n) \sim \frac{1}{2}\left[\frac{1}{i\nu_n + \mu - \varepsilon_d + t - \Sigma^{\sigma}_A(i\nu_n)} + \frac{1}{i\nu_n + \mu - \varepsilon_d - t - \Sigma^{\sigma}_A(i\nu_n)}\right].$$

5. Calculate a new bath Green function $\mathcal{G}^{\sigma}_{i,i}(i\nu_n)$ from the local Dyson equation

$$\mathcal{G}^{\sigma}_{i,i}(i\nu_n) = \frac{1}{\Sigma^{\sigma}_A(i\nu_n) + 1/G^{\sigma}_{i,i}(i\nu_n)}.$$

6. Build a new $G^{0\sigma}_{d,d}(i\nu_n)$ from $\mathcal{G}^{\sigma}_{i,i}(i\nu_n)$.

7. Restart from the second step.

8. Iterate till self-consistency, i.e., here till $n^{\sigma}_d = n^{\sigma}_i$ and $\Sigma^{\sigma}_A(i\nu_n)$ does not change any more.

The Anderson molecule satisfies the self-consistency requirements for $\varepsilon_s = \mu$. The remaining difference between $G^{\sigma}_{d,d}(i\nu_n)$, the impurity Green function, and $G^{\sigma}_{i,i}(i\nu_n)$, the local Green function of the Hubbard dimer in the local self-energy approximation, arises from the difference in the associated hybridization functions

$$\Delta\mathcal{F}_l(i\nu_n) = \mathcal{F}^{\sigma}_l(i\nu_n) - \mathcal{F}^{\sigma}_0(i\nu_n) = t^2p^2\left(-\frac{2}{i\nu_n} + \frac{1}{i\nu_n - \varepsilon_a} + \frac{1}{i\nu_n + \varepsilon_a}\right)$$

where $p^2 = U^2/8\varepsilon_a^2$ and $\varepsilon_a = \sqrt{9t^2 + U^2/4}$. If we use the Anderson molecule as quantum-impurity model we neglect $\Delta\mathcal{F}_l(i\nu_n)$; the error made is small, as shown in the left panels of Fig. 1. To further improve we would have to modify the auxiliary model adding more bath sites. Remaining with the Anderson molecule, let us compare in more detail its spectral function with the exact spectral function of the Hubbard dimer. Fig. 2 shows that the evolution as a function of U is different for the two Hamiltonians. Anticipating the discussion of next session, if we compare to the spectral function of the actual lattice Hubbard model, we could say that the Anderson molecule partially captures the behavior of the central "quasi-particle" or "Kondo"

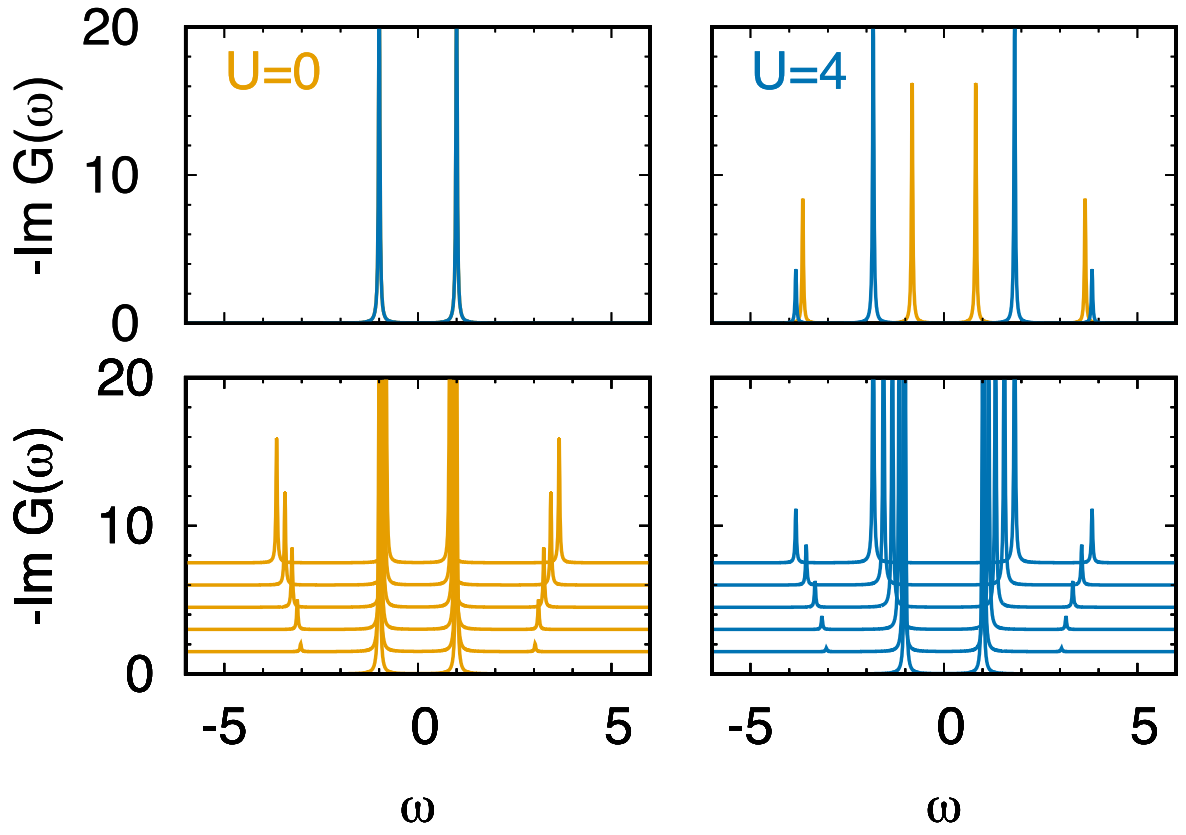

Fig. 2: *Imaginary part of the Green function of the Anderson molecule (orange) and Hubbard dimer (blue) in the zero temperature limit. For the Hubbard dimer the exact Green functions are used, as in the right panels of Fig. 1. Parameters:* $t = 1$, $\varepsilon_s = \mu$. *Top:* $U = 0$ *(left) and* $U = 4t$ *(right). Bottom: evolution with increasing* U *from* 0 *to* $4t$ *in equal steps.*

peak with increasing U, although the Kondo effect itself is unrealistically described; as a matter of fact, the Kondo energy gain (the "Kondo temperature") is perturbative ($\propto t^2/U$) in the case of the Anderson molecule, while it is exponentially small for a Kondo impurity in a metallic bath. On the other hand, the Hubbard dimer captures well the Hubbard bands and the gap in the large-U limit. The example of the Anderson molecule also points to the possible shortcomings of calculations for the lattice Hubbard model (4), in which the DMFT quantum-impurity model is solved via exact diagonalization, however using a single bath site or very few; this might perhaps be sufficient in the limit of large gap,[3] but is bound to eventually fail approaching the metallic regime. Indeed, this failure is one of the reasons why the solution of the Kondo problem required the development of – at the time new – non-perturbative techniques such as the numerical renormalization group.

[3]For a discussion of bath parametrization in exact diagonalization and the actual convergence with the number of bath sites for the lattice Hubbard model see Ref. [9].

2.2 DMFT for the one-band Hubbard model

The Hubbard Hamiltonian (4) is in principle the simplest model for the description of the Mott metal-insulator transition. In the tight-binding approximation it becomes

$$\hat{H} = \varepsilon_d \sum_{\sigma i} \hat{n}_{i\sigma} - t \sum_{\sigma \langle ii' \rangle} c^\dagger_{i\sigma} c_{i'\sigma} + U \sum_i \hat{n}_{i\uparrow} \hat{n}_{i\downarrow}, \tag{7}$$

where $\langle ii' \rangle$ is a sum over first neighbors. For $U = 0$, at half-filling, this Hamiltonian describes a metallic band. For $t = 0$ it describes an insulating collection of disconnected atoms. Somewhere in between, at a critical value of t/U, a metal to insulator transition must occur. In this section we will discuss the DMFT solution of (7) and the picture of the metal-insulator transition emerging from it. The first step consists in mapping the original many-body Hamiltonian into an effective quantum-impurity model, such as the Anderson Hamiltonian

$$\hat{H}^A = \underbrace{\sum_{\boldsymbol{k}\sigma} \varepsilon^s_{\boldsymbol{k}} \hat{n}_{\boldsymbol{k}\sigma}}_{\hat{H}_{\rm bath}} + \underbrace{\sum_{\boldsymbol{k}\sigma} \left(V^s_{\boldsymbol{k}} c^\dagger_{\boldsymbol{k}\sigma} c_{d\sigma} + \text{h.c.} \right)}_{\hat{H}_{\rm hyb}} + \underbrace{\varepsilon_d \sum_\sigma \hat{n}_{d\sigma} + U \hat{n}_{d\uparrow} \hat{n}_{d\downarrow}}_{\hat{H}_{\rm imp}} .$$

In this model the on-site Coulomb repulsion U appears only in the impurity Hamiltonian, $\hat{H}_{\rm imp}$, while the terms $\hat{H}_{\rm bath}$ and $\hat{H}_{\rm hyb}$, describe, respectively, the bath and the bath-impurity hybridization. In the next step, the quantum-impurity model is solved. Differently from the case of the Anderson molecule, this cannot be done analytically. It requires non-perturbative numerical methods, such as exact diagonalization, the numerical renormalization group or quantum Monte Carlo (QMC). Here we describe the DMFT self-consistency loop for a QMC quantum-impurity solver. Solving the quantum-impurity model yields the impurity Green function $G^\sigma_{d,d}(i\nu_n)$. From the impurity Dyson equation we can calculate the impurity self-energy

$$\Sigma^\sigma_A(i\nu_n) = \left(G^{0\sigma}_{d,d}(i\nu_n) \right)^{-1} - \left(G^\sigma_{d,d}(i\nu_n) \right)^{-1}.$$

Next, we adopt the local approximation, i.e., we assume that the self-energy of the Hubbard model equals the impurity self-energy. Then, the local Green function is given by

$$G^\sigma_{i_c,i_c}(i\nu_n) = \frac{1}{N_{\boldsymbol{k}}} \sum_{\boldsymbol{k}} \frac{1}{i\nu_n + \mu - \varepsilon_{\boldsymbol{k}} - \Sigma^\sigma_A(i\nu_n)},$$

where $N_{\boldsymbol{k}}$ is the number of $\boldsymbol{k}$ points. The local Dyson equation is used once more, this time to calculate the bath Green function $\mathcal{G}^\sigma(i\nu_n)$, which in turn defines a new quantum-impurity model. This procedure is repeated until self-consistency is reached, and

$$G^\sigma_{i_c,i_c}(i\nu_n) = G^\sigma_{d,d}(i\nu_n).$$

It is important to underline that self-consistency is key to the success of DMFT in describing the metal-to-insulator transition. This can, perhaps, be best understood looking at a simpler self-consistent method, the static mean-field or Hartree-Fock approach.[4] In the static mean-field

[4] Keeping in mind that many self-consistent solutions obtained with the Hartree-Fock method are spurious.

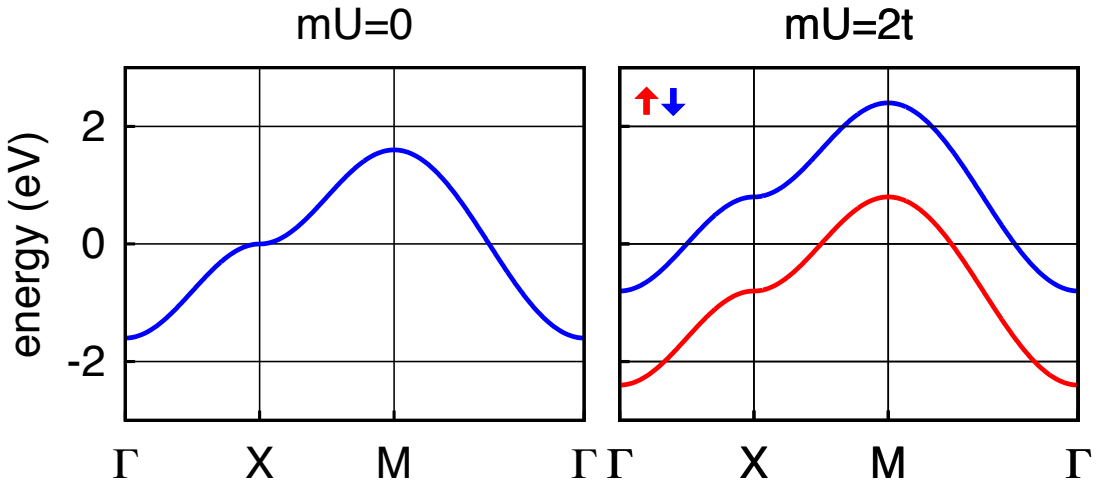

Fig. 3: *The metal-insulator transition in ferromagnetic Hartree-Fock. The calculation is for a square lattice tight-binding model with dispersion* $\varepsilon_{\boldsymbol{k}} = -2t(\cos k_x + \cos k_y)$.

approximation we replace the Coulomb interaction of the Hubbard model (7) with a one-body operator

$$U\hat{n}_{i\uparrow}\hat{n}_{i\downarrow} \longrightarrow U\big(\bar{n}_{i\uparrow}\hat{n}_{i\downarrow} + \hat{n}_{i\uparrow}\bar{n}_{i\downarrow} - \bar{n}_{i\uparrow}\bar{n}_{i\downarrow}\big),$$

where $\bar{n}_{i\sigma}$ is the expectation value of $\hat{n}_{i\sigma}$; for simplicity, here we additionally assume that $\bar{n}_{i\sigma} = \bar{n}_\sigma$. The approximation is then identical to replacing the Hamiltonian with

$$\hat{H}_{\mathrm{MF}} = \sum_{\boldsymbol{k}\sigma} \left[\varepsilon_{\boldsymbol{k}} + U\left(\frac{1}{2} - \sigma m\right)\right]\hat{n}_{\boldsymbol{k}\sigma}, \tag{8}$$

where $\sigma = +1$ for spin up and $\sigma = -1$ for spin down; thus $h_{\mathrm{eff}} = 2Um$ plays the role of an effective field (Weiss field). The self-consistency criterion is simply

$$\bar{n}_\sigma = \langle \hat{n}_\sigma \rangle_{\mathrm{MF}},$$

where the expectation value $\langle \hat{n}_\sigma \rangle_{\mathrm{HF}}$ is calculated using the Hamiltonian $\hat{H}_{\mathrm{HF}}$, which in turn depends on $\bar{n}_\sigma$ via m. This gives the self-consistency equation

$$m = \frac{1}{2}\frac{1}{N_{\boldsymbol{k}}}\sum_{\boldsymbol{k}\sigma} \frac{\sigma e^{-\beta[\varepsilon_{\boldsymbol{k}} + U(\frac{1}{2} - \sigma m) - \mu]}}{1 + e^{-\beta[\varepsilon_{\boldsymbol{k}} + U(\frac{1}{2} - \sigma m) - \mu]}}.$$

If we set $m = 0$ the equation is satisfied; for such a trivial solution the static mean-field correction in Eq. (8) merely redefines the chemical potential and has therefore no effect. For sufficiently large U, however, a non-trivial solution ($m \neq 0$) can be found. If $m \neq 0$ the spin up and spin down bands split, and eventually a gap can open. This is shown in Fig. (3). The static mean-field correction in Eq. (8) equals the contribution of the Hartree diagram to the self-energy, $\Sigma^\sigma_{\mathrm{H}}(i\nu_n) = U\bar{n}_{-\sigma}$. In many-body perturbation theory, however, $\bar{n}_\sigma = 1/2$, i.e., $m = 0$. In the self-consistent static mean-field approximation, instead, m can differ from zero, and a

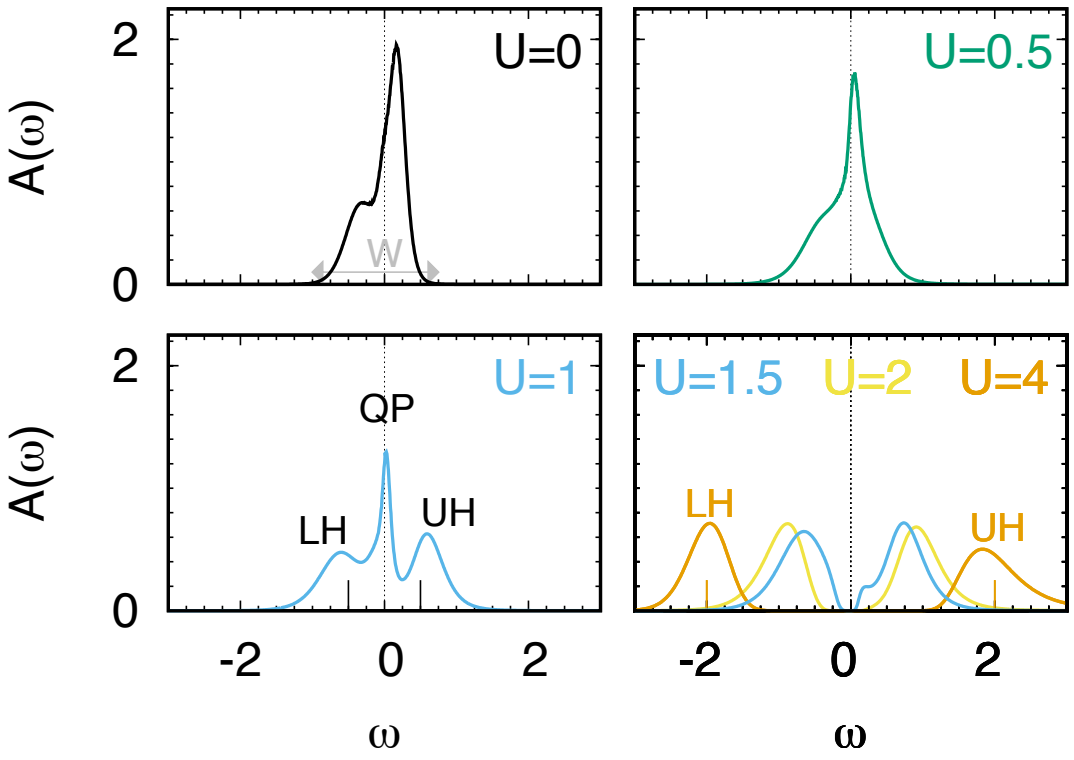

Fig. 4: *$VOMoO_4$: LDA+DMFT spectral function at finite temperature for $0 \leq U \leq 4$. Energies are in eV and spectral functions in states/spin/eV. The calculations have been done using a continuous-time hybridization-expansion QMC solver [10]. A detailed LDA+DMFT study of the electronic and magnetic properties $VOMoO_4$ can be found in Ref. [11].*

phenomenon not described by the mere Hartree diagram can be captured, ferromagnetism in a correlated metal. In DMFT the role of the Weiss field is played by the bath Green function $\mathcal{G}^{\sigma}_{i,i}(i\nu_n)$. The emerging picture of the Mott transition is described in Fig. 4 for a representative single-band material. In the $U = 0$ limit, the spectral function $A_0(\omega)$ is metallic at half filling (top left panel). For finite U, if we set $\Sigma^{\sigma}_A(\omega) = 0$ as initial guess, the DMFT self-consistency loop starts with $A(\omega) = A_0(\omega)$. For small U/t, the *converged* spectral function $A(\omega)$ is still similar to $A_0(\omega)$. This can be seen comparing the $U = 0.5$ and $U = 0$ panels in Fig. 4. Further increasing U/t, sizable spectral weight is transferred from the zero-energy quasi-particle peak to the lower (LH) and upper (UH) Hubbard bands, centered at $\omega \sim \pm U/2$. This can be observed in the $U = 1$ panel of Fig. 4. The system is still metallic, but with strongly renormalized masses and short lifetimes, reflected in the narrow quasi-particle (QP) peak. Finally, for U larger than a critical value ($U \geq 1.5$ in the figure) a gap opens and the system is a Mott insulator. When this happens the self-energy diverges at low frequency, where

$$\Sigma^{\sigma}_A(\omega + i0^+) \sim \frac{U}{2} + \frac{A}{\omega + i0^+}.$$

In the large U/t limit the gap increases linearly with the Coulomb repulsion, i.e., $E_g(1) \sim U - W$, where W is the bandwidth.

2.3 DMFT for multi-orbital models

The multi-orbital Hubbard-like Hamiltonian has the form

$$\begin{aligned}\hat{H} &= \hat{H}_0 + \hat{H}_U \\ \hat{H}_0 &= -\sum_{ii'}\sum_{\sigma}\sum_{mm'} t^{i,i'}_{m\sigma,m'\sigma'}\, c^{\dagger}_{im\sigma} c_{i'm'\sigma'} \\ \hat{H}_U &= \frac{1}{2}\sum_{i}\sum_{\sigma\sigma'}\sum_{mm'}\sum_{pp'} U_{mpm'p'}\, c^{\dagger}_{im\sigma} c^{\dagger}_{ip\sigma'} c_{ip'\sigma'} c_{im'\sigma},\end{aligned}$$

where m, m' and p, p' are different orbitals and the Coulomb tensor is local. The DMFT approach can be extended to solve models of this form, mapping them to multi-orbital quantum-impurity models. The main changes with respect to the formalism introduced in the previous section are then the following

$$\begin{aligned} \varepsilon_{\boldsymbol{k}} &\to (H_{\boldsymbol{k}})_{m\sigma,m'\sigma'} & (i\nu_n + \mu) &\to (i\nu_n + \mu)\hat{1}_{m\sigma,m'\sigma'} \\ t^{i,i'} &\to t^{i,i'}_{m\sigma,m'\sigma'} & \varepsilon_d &\to \varepsilon^{i,i'}_{m\sigma,m'\sigma'} = -t^{i,i}_{m\sigma,m'\sigma'} \end{aligned}$$

where $\hat{1}$ is the unity matrix. As a consequence, the local Green function, the bath Green function, the hybridization function and the self-energy also become matrices in spin-orbital space

$$\mathcal{G}^{\sigma}(i\nu_n) \to \mathcal{G}^{\sigma,\sigma'}_{m,m'}(i\nu_n) \qquad G^{\sigma}(i\nu_n) \to G^{\sigma,\sigma'}_{m,m'}(i\nu_n) \qquad \Sigma^{\sigma}(i\nu_n) \to \Sigma^{\sigma,\sigma'}_{m,m'}(i\nu_n).$$

The corresponding generalization of the self-consistency loop is shown schematically in Fig. 5. Although the extension of DMFT to Hubbard models with many orbitals might appear straightforward, in practice it is not. The bottleneck is the solution of the generalized multi-orbital quantum-impurity problem. The most flexible solvers available so far are all based on QMC. Despite being flexible, QMC-based approaches have limitations. These can be classified in two types. First, with increasing the number of degrees of freedom, calculations become very quickly computationally too expensive – how quickly depends on the specific QMC algorithm used and the actual implementation. Thus, going beyond a rather small number of orbitals and reaching the zero-temperature limit is unfeasible in practice. The second type of limitation is more severe. Increasing the number of degrees of freedom leads, eventually, to the infamous sign problem; when this happens, QMC calculations cannot be performed at all. In order to deal with limitations of the first type, it is crucial to restrict QMC calculations to the essential degrees of freedom; furthermore, we should exploit symmetries, develop fast algorithms and use the power of massively parallel supercomputers to reduce the actual computational time. For the second type of problems not a lot can be done; nevertheless, it has been shown that a severe sign problem might appear earlier with some basis choices than with others [10]. Although eventually we cannot escape it, this suggests that the model set up can be used as a tool to expand the moderate sign-problem zone. For what concerns symmetries, in the paramagnetic case and in absence of spin-orbit interaction or external fields, an obvious symmetry to exploit

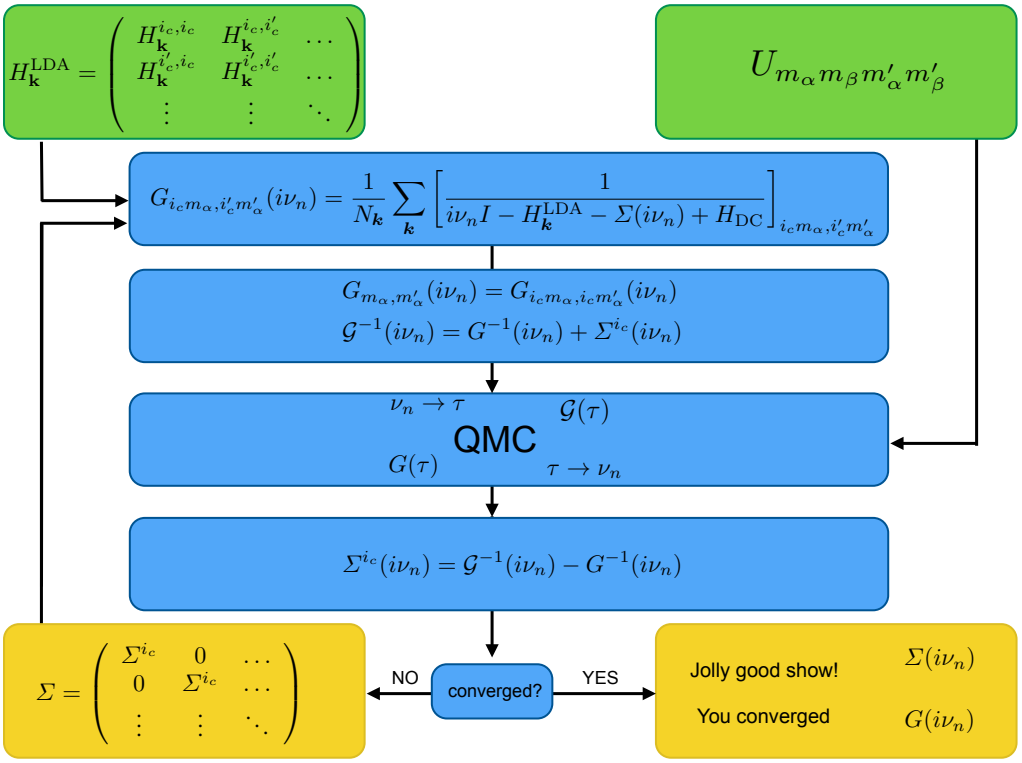

Fig. 5: *LDA+DMFT self-consistency loop. The one-electron Hamiltonian is built in the basis of Bloch states obtained from localized Wannier functions, for example in the local-density approximation (LDA); this gives* $H^{\rm LDA}_{\boldsymbol{k}}$. *The set* $\{i_c\}$ *labels the equivalent correlated sites inside the unit cell. The local Green-function matrix is at first calculated using an initial guess for the self-energy matrix. The bath Green-function matrix is then obtained via the Dyson equation and used to construct an effective quantum-impurity model. The latter is solved via a quantum-impurity solver, here quantum Monte Carlo (QMC). This yields the impurity Green-function matrix. Through the Dyson equation the self-energy is then obtained, and the procedure is repeated until self-consistency is reached.*

is the $SO(3)$ rotational invariance of spins, from which follows

$$A^{\sigma,\sigma'}_{m,m'}(i\nu_n) = \delta_{\sigma,\sigma'}\, A_{m,m'}(i\nu_n),$$

where $A = \mathcal{G}, G, \Sigma$. In addition, if we use a basis of real functions, the local Green-function matrices are real and symmetric in imaginary time τ, hence

$$A^{\sigma,\sigma'}_{m,m'}(\tau) = \delta_{\sigma,\sigma'}\, A_{m,m'}(\tau) = \delta_{\sigma,\sigma'}\, A_{m',m}(\tau).$$

Finally, often the unit cell contains several equivalent correlated sites, indicated as $\{i_c\}$ in Fig. 5. In order to avoid expensive cluster calculations, we can use space-group symmetries to construct the matrices $\mathcal{G}, G, \Sigma$ at a given site i'_c from the corresponding matrices at an equivalent site, e.g., $i_c = 1$. Space-group symmetries also tell us if some matrix elements are zero. For example, for a model with only t_{2g} (or only e_g) states, in cubic symmetry, in the paramagnetic case and in absence of spin-orbit interaction or external fields, we have

$$A^{\sigma,\sigma'}_{m,m'}(\tau) = \delta_{\sigma,\sigma'}\, A_{m,m}(\tau)\, \delta_{m,m'}.$$

2.4 Minimal material-specific models from LDA

How do we build realistic Hubbard-like models for correlated materials? The state-of-the art approach relies on constructing, for a given system, *material-specific* Wannier functions. The latter can be obtained via electronic structure calculations based on density-functional theory (DFT) [12, 13]. If we construct a complete basis of Wannier functions, the complete many-body Hamiltonian takes the form that we have seen in the introduction, $\hat{H} = \hat{H}_0 + \hat{H}_U$, with

$$\hat{H}_0 = \hat{H}^{\rm LDA} = -\sum_{\sigma} \sum_{ii'} \sum_{mm'} t^{i,i'}_{m,m'} c^{\dagger}_{im\sigma} c_{i'm'\sigma},$$

$$\hat{H}_U = \frac{1}{2} \sum_{ii'jj'} \sum_{\sigma\sigma'} \sum_{mm'pp'} U^{iji'j'}_{mp\,m'p'} c^{\dagger}_{im\sigma} c^{\dagger}_{jp\sigma'} c_{j'p'\sigma'} c_{i'm'\sigma}.$$

The potential entering in the hopping integrals, Eq. (3), is given by the self-consistent DFT reference potential

$$v_{\rm R}(\boldsymbol{r}) = v_{\rm en}(\boldsymbol{r}) + v_{\rm H}(\boldsymbol{r}) + v_{\rm xc}(\boldsymbol{r}) = -\sum_{\alpha} \frac{Z_\alpha}{|\boldsymbol{r} - \boldsymbol{R}_\alpha|} + \int d\boldsymbol{r}' \, \frac{1}{|\boldsymbol{r} - \boldsymbol{r}'|} + v_{\rm xc}(\boldsymbol{r}).$$

The formula above shows that $v_{\rm R}(\boldsymbol{r})$ includes Coulomb effects, via the long-range Hartree term $v_{\rm H}(\boldsymbol{r})$ and the exchange-correlation contribution $v_{\rm xc}(\boldsymbol{r})$; for the latter we use, e.g., the LDA approximation. Thus in our Hamiltonian some Coulomb effects are included both in $\hat{H}_0$, via $v_{\rm R}(\boldsymbol{r})$, and in $\hat{H}_U$. In order to avoid double counting, we have then to subtract from $\hat{H}_U$ the effects already included in $\hat{H}_0$. Thus we have to replace

$$\hat{H}_U \to \Delta\hat{H}_U = \hat{H}_U - \hat{H}_{\rm DC},$$

where $\hat{H}_{\rm DC}$ is the so-called double-counting correction. Unfortunately we do not know which correlation effects are indeed included in $\hat{H}_0$ via the LDA reference potential, and therefore the exact expression of $\hat{H}_{\rm DC}$ is also unknown. The remarkable successes of the LDA suggest, however, that in many materials the LDA is overall a good approximation, and therefore, in those systems at least, the term $\Delta\hat{H}_U$ can be completely neglected. What about strongly-correlated materials? Even in correlated systems, most likely the LDA works rather well for the delocalized electrons or in describing the average or the long-range Coulomb effects. Thus one can think of separating the electrons into *uncorrelated* and *correlated*; only for the latter we do take the correction $\Delta\hat{H}_U$ into account explicitly, assuming furthermore that $\Delta\hat{H}_U$ is local or almost local [12]. Typically, correlated electrons are those that partially retain their atomic character, e.g., those that originate from localized d and f shells; for convenience, here we assume that in a given system they stem from a single atomic shell l (e.g., d for transition-metal oxides or f for heavy-fermion systems) and label their states with the atomic quantum numbers l and $m = -l, \ldots, l$ of that shell. Thus

$$U^{iji'j'}_{mp\,m'p'} \sim \begin{cases} U^{l}_{mp\,m'p'} & iji'j' = iiii \quad \wedge \quad mp, m'p' \in l \\ 0 & iji'j' \neq iiii \quad \vee \quad mp, m'p' \notin l. \end{cases}$$

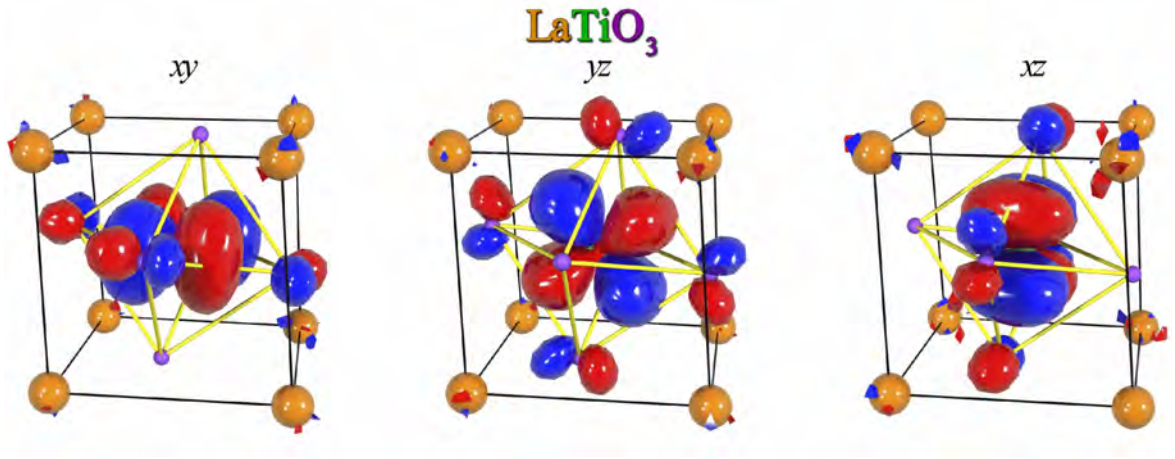

Fig. 6: *NMTO Wannier-like orbitals for t_{2g} states in LaTiO$_3$ obtained via massive downfolding to the t_{2g} bands. The t_{2g}-like orbitals have O p tails at the neighboring O sites reflecting the distortions of the lattice. The figure has been taken from Ref. [14].*

Within this approximation $\Delta\hat{H}_U$ is replaced by $\Delta\hat{H}^l_U = \hat{H}^l_U - \hat{H}^l_{\rm DC}$, where $\hat{H}^l_{\rm DC}$ is, e.g., given by the static mean-field contribution of $\hat{H}^l_U$. There is a drawback in this procedure, however. By splitting electrons into correlated and uncorrelated we implicitly assume that the main effect of the latter is the renormalization or *screening* of parameters for the former, in particular of the Coulomb interaction. The computation of screening effects remains, unfortunately, a challenge. The calculation of exact screening would require the (impossible) solution of the original many-body problem, taking all degrees of freedom into account. Commonly-used approximate schemes are the constrained LDA approximation (cLDA) and the constrained random-phase approximation (RPA) [12, 13]. Both methods give reasonable estimates of screened Coulomb parameters for DMFT calculations. Typically cRPA calculations include more screening channels and are performed for less localized bases than cLDA calculations; thus cRPA parameters turn out to be often smaller than cLDA ones. To some extent, the difference can be taken as an estimate of the error bar. After we have selected the electrons for which we think it is necessary to include explicitly the Hubbard correction, in order to build the final Hamiltonian for DMFT calculations, it is often convenient to integrate out or *downfold*, in part or completely, the weakly correlated states. There are different degrees of downfolding. The two opposite extreme limits are (i) *no downfolding*, i.e., keep explicitly in the Hamiltonian all weakly-correlated states (ii) *massive downfolding*, i.e., downfold all weakly correlated states. If we perform massive downfolding, e.g., downfold to the d (or e_g or t_{2g}) bands at the Fermi level, the Hamiltonian relevant for DMFT takes a simpler form. The LDA part is limited to the selected orbitals or bands, which, in the ideal case, are decoupled from the rest

$$\hat{H}^{\rm LDA} = -\sum_{\sigma}\sum_{ii'}\sum_{m_\alpha m'_\alpha} t^{i,i'}_{m_\alpha,m'_\alpha}\, c^\dagger_{im_\alpha\sigma}\, c_{i'm'_\alpha\sigma}.$$

The local *screened* Coulomb interaction for this set of orbitals is the on-site tensor

$$\hat{H}_U^l = \frac{1}{2}\sum_i \sum_{\sigma\sigma'} \sum_{m_\alpha m'_\alpha} \sum_{m_\beta m'_\beta} U_{m_\alpha m_\beta m'_\alpha m'_\beta}\, c^\dagger_{im_\alpha\sigma} c^\dagger_{im_\beta\sigma'} c_{im'_\beta\sigma'} c_{im'_\alpha\sigma}.$$

It is important to point out that the level of downfolding does not modify the hardness of the quantum-impurity problem. If, for example, in studying a transition-metal oxide, we plan to treat only $3d$ bands as correlated, it does not matter if we perform calculations with a Hamiltonian containing also, e.g., O p states, or we rather downfold all states but the $3d$ and work with a set of Wannier basis spanning the $3d$-like bands only. The number of correlated orbitals in the quantum-impurity problem is the same.[5] One advantage of massive downfolding is that the double-counting correction typically becomes a shift of the chemical potential, and it is therefore not necessary to calculate it explicitly. A second important advantage is that the interpretation of the final results is simpler. Instead, a disadvantage is that the basis functions are less localized, and therefore the approximation of the Coulomb interaction to a local operator might be less justified, and in some cases it might be necessary to include non-local Coulomb terms. The effect of downfolding on the localization of Wannier functions is illustrated for example in Fig. 6. Considered all advantages and disadvantages, what is then the best way of performing DMFT calculations? There is no universal answer to this question; it depends on the problem we are trying to solve and the system we are studying. Independently on the degree of downfolding we chose, it is important to point out that a clear advantage of Wannier functions in general is that they carry information about the lattice, bonding, chemistry and distortions. This can be seen once more in Fig. 6, where orbitals are tilted and deformed by the actual structure and chemistry of the compound. Indeed, one might naively think of using an "universal" basis, for example atomic functions, the same for all systems. Apart the complications arising from the lack of orthogonality, such a basis has no built-in material-specific information, except lattice positions. It is therefore a worse starting point to describe the electronic structure, even in the absence of correlations; larger basis sets are required to reach the same accuracy. From the point of view of LDA+DMFT, an advantage of an universal basis would be that it is free from double-counting corrections; on the other hand, however, exactly because we do not use the LDA potential to calculate the hopping integrals, we also cannot count on the successes of LDA in the description of average and long-range Coulomb effects. For these reasons *ab-initio* Wannier functions remain so far the basis of choice. They can be built via the Nth-Order Muffin-Tin Orbital (NMTO) method [14], the maximal-localization scheme [15] or projectors. Fig. 6 shows examples of NMTO-based Wannier functions.

No matter what construction procedure is used, a common characteristic of *ab-initio* Wannier functions is that they are site-centered and localized.[6] Thus a question naturally arises: How important is it to use localized functions as one-electron basis? In the extreme limit in which the basis functions are independent of the lattice position (i.e., they are totally delocalized), the

[5] The choice might influence how severe the QMC sign problem is, however.

[6] Differences in localizations between the various construction procedures are actually small for the purpose of many-body calculations, provided that the same bands are spanned in the same way.

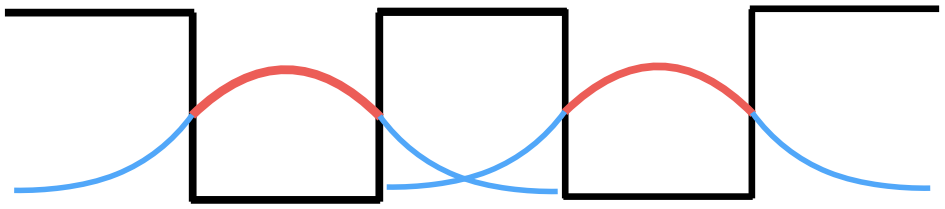

Fig. 7: *The problem of two quantum wells. The figure shows (schematically) for each well the wavefunction of a bound state. If we consider only the part of the wavefunction inside its own well (red in the figure), the differential overlap (and hence the hopping integral) between functions centered on different wells would be zero.*

Coulomb interaction parameters would be the same for every couple of lattice sites, no matter how distant. Thus a Hubbard-like model would be hard to justify. In the other extreme case, we could, hypothetically, adopt a basis so localized that $\psi_{im\sigma}(\boldsymbol{r})\overline{\psi_{i'm'\sigma'}}(\boldsymbol{r}) \sim \delta_{i,i'}\delta(\boldsymbol{r}-\boldsymbol{T}_i)$. Even for such a basis, the unscreened Coulomb interaction is not local. It is given by

$$U^{iji'j'}_{mp\,m'p'} \propto \frac{\delta_{i,i'}\delta_{j,j'}}{|\boldsymbol{T}_i - \boldsymbol{T}_j|},$$

hence it decays slowly with distance, although the (divergent) on-site term dominates. More generally, we can conclude that by increasing the localization of the basis we enhance the importance of the on-site Coulomb repulsion with respect to long-range terms; this better justifies Hubbard-like models. The example illustrates also how far we can go. A major problem with the basis discussed above is that it would be impossible to properly describe bonding, since the hopping integrals would be zero. Although such a basis is, of course, never used to build many-body models, there is a tempting approximation that has similar flaws. If one uses DFT-based electronic-structure techniques that tile the space in interstitial and non-overlapping atomic spheres (e.g., the LAPW method), it is tempting to use as basis for correlated electrons the atomic functions defined inside the atomic spheres. These functions are, by construction, much more localized than Wannier orbitals (even if no downfolding is performed in the Wannier construction). However, they do not form a complete basis set in the space of square-integrable functions. This is obvious because such a basis does not even span the LDA bands; to reproduce the bands we need, in addition, functions defined in the interstitial region. This is illustrated in Fig. 7 for a simple example of two quantum well potentials.[7] We therefore cannot use it to write the many-body Hamiltonian in the usual form $\hat{H}_0 + \hat{H}_U$. In conclusion, a basis which, as *ab-initio* Wannier functions, is complete and indeed spans the bands, is better justified, although we somewhat lose in localization.

[7] Another, but less severe, problem of atomic sphere truncations is that the results will depend on the sphere size, in particular when atomic spheres are small.

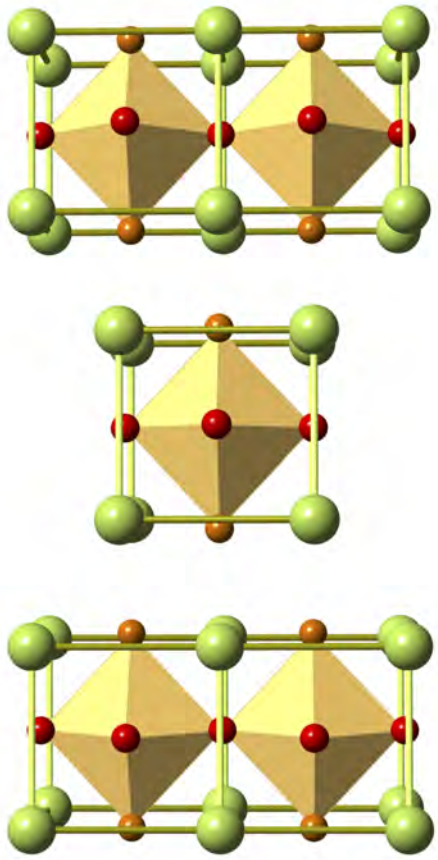

Fig. 8: *The crystal structure of the tetragonal layered perovskite Sr_2RuO_4. The figure has been adapted from Ref. [16].*

3 Multi-orbital Hubbard models

In this section we will discuss some of the specific effects emerging in multi-orbital Hubbard models, pointing out the differences with respect to the case of the one-band Hubbard model. As examples we will use perovskites with partially filled t_{2g} shells. A representative system of this kind is Sr_2RuO_4, whose layered crystal structure is shown in Fig. 8. The LDA bands of Sr_2RuO_4 around the Fermi level ($4d\ t_{2g}^4$ configuration) are shown in Fig. 9. The figure shows the $4d\ t_{2g}$ bands crossing the Fermi level, in red the xz, yz bands and in blue the xy band. Due to the layered structure, the xz and yz bands are quasi one-dimensional and the xy band is quasi two-dimensional. Thus, they give rise, in first approximation, to a Fermi surface made of four crossing lines (from the xz, yz bands) and a circle (from the xy band). This is shown schematically in the left panel of Fig. 9. Experimentally, Sr_2RuO_4 is a correlated metal down to 1.5 K; below this temperature it becomes an anomalous superconductor. The two other examples considered in this lecture are orbitally ordered Mott insulators. The first is

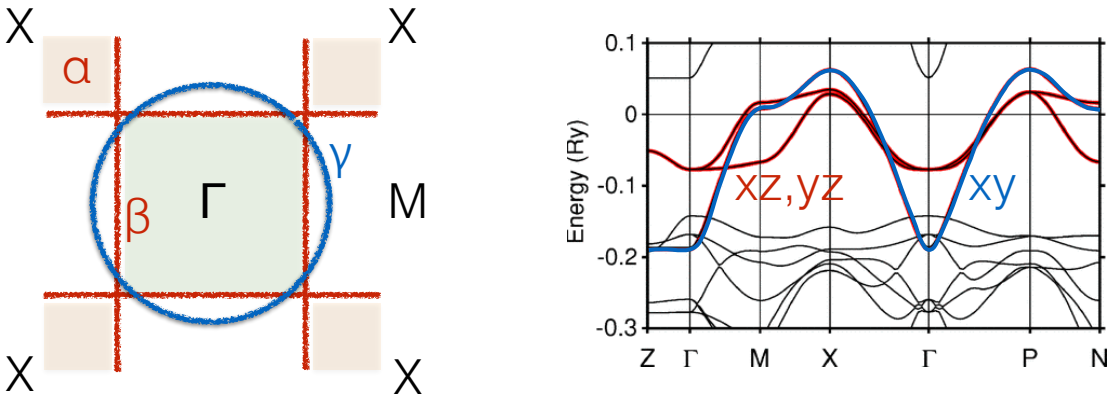

Fig. 9: *Schematic representation of the Fermi surface of the tetragonal t_{2g}^4 system Sr_2RuO_4 (left) and the associated LDA band structure (right). The figure is rearranged from Ref. [16]. The band structure was calculated using the Nth-Order Muffin-Tin Orbital (NMTO) method.*

Ca_2RuO_4, isoelectronic and very similar to Sr_2RuO_4, except that its crystal symmetry is lower than tetragonal. The second is the 3-dimensional orthorhombic perovskite $YTiO_3$, with the electronic configuration $3d\, t_{2g}^1$. For all these materials, if we massively downfold all bands but the t_{2g}, the associated 3-band Hubbard model becomes

$$\begin{aligned}\hat{H} =& \sum_{i\sigma}\sum_{mm'} \varepsilon_{m,m'}\, c^\dagger_{im\sigma} c_{im'\sigma} - \sum_{\sigma}\sum_{i\neq i'}\sum_{mm'} t^{i,i'}_{m,m'}\, c^\dagger_{im\sigma} c_{i'm'\sigma} \\ &+ U \sum_{i\, m} \hat{n}_{im\uparrow}\hat{n}_{im\downarrow} + \frac{1}{2}\sum_{\substack{i\sigma\sigma' \\ m\neq m'}} \left(U - 2J - J\delta_{\sigma,\sigma'}\right) \hat{n}_{im\sigma}\hat{n}_{im'\sigma'} \\ &- J \sum_{i\; m\neq m'} \left(c^\dagger_{im\uparrow} c^\dagger_{im\downarrow} c_{im'\uparrow} c_{im'\downarrow} + c^\dagger_{im\uparrow} c_{im\downarrow} c^\dagger_{im'\downarrow} c_{im'\uparrow} \right),\end{aligned}$$

where $m, m' = xy, yz, xz$, and where U and J are the direct and exchange screened Coulomb integrals for t_{2g} electrons. The Coulomb interaction $\hat{H}_U$ is here assumed to have full $O(3)$ rotational symmetry, as in the atomic limit.[8] The first two terms of $\hat{H}_U$ are the so-called density-density terms, and the last two are the pair-hopping and spin-flip interaction. In the Hamiltonian above we dropped the double-counting correction $\hat{H}_{\rm DC}$, which in this case is a mere shift of the chemical potential, as we will see later. The energies $\varepsilon_{m,m'}$ are the crystal-field matrix, and thus, in principle, in the atomic limit $\varepsilon_{m,m'} = \varepsilon_d\, \delta_{m,m'}$. In the following sections we will however consider as atomic limit the case in which only the hopping integrals $t^{i,i'}_{m,m'}$ are zero.

[8] For the derivation of the Coulomb interaction $\hat{H}_U$ for t_{2g} electrons starting from the complete Coulomb tensor of the free atom, see my chapter in Ref. [12].

3.1 Atomic limit, multiplets and cubic crystal field

Let us start considering the atomic limit. For the one-band Hubbard model, in the atomic limit, the local spectral function at half filling (d^1 electronic configuration) is given by

$$G^{\sigma}_{ii}(i\nu_n) = \frac{1}{2}\left[\frac{1}{i\nu_n - (\underbrace{\varepsilon_d - \mu}_{E(N)-E(N-1)-\mu})} + \frac{1}{i\nu_n - (\underbrace{\varepsilon_d + U - \mu}_{E(N+1)-E(N)-\mu})}\right]$$

with $\mu = \varepsilon_d + U/2$. The gap is $E_g(1) = U$ and the spectral function displays a lower and an upper Hubbard peaks, located at energy $\pm U/2$. In the presence of many orbitals, the Hubbard peaks acquire a complicated structure. This is due to the fact that the eigenstates of the Coulomb matrix for a given number of electrons form multiplets with different energies. For the d^n configuration there are three independent Coulomb parameters on which the energy of a multiplet depends: the direct term U, the Hund's rule exchange coupling for t_{2g} electrons, $J{=}J_1$, and the Hund's rule exchange coupling for e_g electrons, J_2. For a free atom (symmetry $O(3)$), the ground multiplet is determined by the three Hund's rules. The first of these rules says that the ground state has the maximum possible total spin S. Thus, for configuration d^4, the ground multiplet has $S{=}2$. Let us call $-\Delta_H$ the Hund's rule energy gain, i.e., the energy difference between the ground and the first excited spin multiplet; Δ_H is a function of J_1 and J_2 and is zero for $J_1 = J_2 = 0$. In cubic symmetry, the crystal field splits e_g and t_{2g} states, and $\varepsilon_C{=}\varepsilon_{e_g}{-}\varepsilon_{t_{2g}}{>}0$; if ε_C is very large, the first Hund's rule can be violated. In $LaMnO_3$, where the energy loss due to ε_C is smaller than Δ_H, the ground multiplet has configuration $t^3_{2g}e^1_g$ and indeed $S{=}2$ (high spin), in line with the first Hund's rule. In Sr_2RuO_4 and Ca_2RuO_4, however, the cubic crystal field prevails, and the ground configuration is $t^4_{2g}e^0_g$, with $S{=}1$ (intermediate spin). Thus, if the crystal field ε_C is large and $n \leq 6$, the e_g orbitals will stay empty, hence, we can restrict the discussion to the t_{2g} orbitals and the $t^n_{2g}e^0_g$ configuration. The energy of the corresponding multiplets are given in Tab. 1, assuming $\varepsilon_{m,m'} = \varepsilon_{t_{2g}}\,\delta_{m,m'}$, and setting for convenience $\varepsilon_{t_{2g}} = 0$. In the t^1_{2g} configuration, the atomic Matsubara Green function is

$$\begin{aligned} G^{\sigma}_{m}(i\nu_n) = & \frac{1}{6}\left[\frac{1}{i\nu_n + (\varepsilon_{t_{2g}} - \mu)} + \frac{3}{i\nu_n - (\varepsilon_{t_{2g}} + U - 3J - \mu)}\right. \\ & \left. + \frac{5/3}{i\nu_n - (\varepsilon_{t_{2g}} + U - J - \mu)} + \frac{1/3}{i\nu_n - (\varepsilon_{t_{2g}} + U + 2J - \mu)}\right], \end{aligned} \tag{9}$$

and it is the same for all orbitals. The associated spectral function has one peak corresponding to $E(1) - E(0) - \mu$. This happens because there is only one state with zero electrons, the vacuum. Instead, there are three peaks corresponding to energy $E(2) - E(1) - \mu$; they are associated with different multiplets of the t^2_{2g} configuration (Fig. 10). The atomic gap takes the value $E_g(1) = U - 3J$, i.e., it is smaller than in the case $J = 0$ and it is smaller than in the one-orbital case. This expression of the atomic gap is also valid for other configurations, t^2_{2g}, t^4_{2g}, and t^5_{2g}. Instead, at half filling (t^3_{2g}), the atomic gap is $E_g(3) = U + 2J$, i.e., it is enhanced and not reduced by J. This can be easily verified by using Tab. 1.

$\|N;S,m_S\rangle$		$E(N,S)$
$\|0\rangle$		
$\|1;\frac{1}{2},\frac{\sigma}{2}\rangle$	$= c^\dagger_{m\sigma}\|0\rangle$	
$\|2;0,0\rangle_a$	$= \frac{1}{\sqrt{3}}\left[c^\dagger_{xz\uparrow}c^\dagger_{xz\downarrow}+c^\dagger_{yz\uparrow}c^\dagger_{yz\downarrow}+c^\dagger_{xy\uparrow}c^\dagger_{xy\downarrow}\right]\|0\rangle$	$U+2J$
$\|2;0,0\rangle_b$	$= \frac{1}{\sqrt{6}}\left[c^\dagger_{xz\uparrow}c^\dagger_{xz\downarrow}+c^\dagger_{yz\uparrow}c^\dagger_{yz\downarrow}-2c^\dagger_{xy\uparrow}c^\dagger_{xy\downarrow}\right]\|0\rangle$	$U-J$
$\|2;0,0\rangle_c$	$= \frac{1}{\sqrt{2}}\left[c^\dagger_{xz\uparrow}c^\dagger_{xz\downarrow}-c^\dagger_{yz\uparrow}c^\dagger_{yz\downarrow}\right]\|0\rangle$	$U-J$
$\|2;1,\sigma,m''\rangle$	$= c^\dagger_{m\sigma}c^\dagger_{m'\sigma}\|0\rangle$	$U-3J$
$\|2;1,0,m''\rangle$	$= \frac{1}{\sqrt{2}}\left[c^\dagger_{m\uparrow}c^\dagger_{m'\downarrow}+c^\dagger_{m\downarrow}c^\dagger_{m'\uparrow}\right]\|0\rangle$	$U-3J$
$\|2;0,0,m''\rangle$	$= \frac{1}{\sqrt{2}}\left[c^\dagger_{m\uparrow}c^\dagger_{m'\downarrow}-c^\dagger_{m\downarrow}c^\dagger_{m'\uparrow}\right]\|0\rangle$	$U-J$
$\|3;\frac{3}{2},\frac{3\sigma}{2}\rangle$	$= c^\dagger_{xz\sigma}c^\dagger_{yz\sigma}c^\dagger_{xy\sigma}\|0\rangle$	$3U-9J$
$\|3;\frac{3}{2},\frac{\sigma}{2}\rangle$	$= \frac{1}{\sqrt{3}}\left[c^\dagger_{xz\sigma}c^\dagger_{yz\sigma}c^\dagger_{xy-\sigma}+c^\dagger_{xz\sigma}c^\dagger_{yz-\sigma}c^\dagger_{xy\sigma}+c^\dagger_{xz-\sigma}c^\dagger_{yz\sigma}c^\dagger_{xy\sigma}\right]\|0\rangle$	$3U-9J$
$\|3;\frac{1}{2},\frac{\sigma}{2}\rangle_a$	$= \frac{1}{\sqrt{6}}\left[-2c^\dagger_{xz\sigma}c^\dagger_{yz\sigma}c^\dagger_{xy-\sigma}+c^\dagger_{xz\sigma}c^\dagger_{yz-\sigma}c^\dagger_{xy\sigma}+c^\dagger_{xz-\sigma}c^\dagger_{yz\sigma}c^\dagger_{xy\sigma}\right]\|0\rangle$	$3U-6J$
$\|3;\frac{1}{2},\frac{\sigma}{2}\rangle_b$	$= \frac{1}{\sqrt{2}}\left[c^\dagger_{xz\sigma}c^\dagger_{yz-\sigma}-c^\dagger_{xz-\sigma}c^\dagger_{yz\sigma}\right]c^\dagger_{xy\sigma}\|0\rangle$	$3U-6J$
$\|3;\frac{1}{2},\frac{\sigma}{2},m\rangle_a$	$= \frac{1}{\sqrt{2}}\left[c^\dagger_{m'\uparrow}c^\dagger_{m'\downarrow}+c^\dagger_{m''\uparrow}c^\dagger_{m''\downarrow}\right]c^\dagger_{m\sigma}\|0\rangle$	$3U-4J$
$\|3;\frac{1}{2},\frac{\sigma}{2},m\rangle_b$	$= \frac{1}{\sqrt{2}}\left[c^\dagger_{m'\uparrow}c^\dagger_{m'\downarrow}-c^\dagger_{m''\uparrow}c^\dagger_{m''\downarrow}\right]c^\dagger_{m\sigma}\|0\rangle$	$3U-6J$
$\|4;1,\sigma,m''\rangle$	$= c^\dagger_{m\sigma}c^\dagger_{m'\sigma}c^\dagger_{m''\uparrow}c^\dagger_{m''\downarrow}\|0\rangle$	$6U-13J$
$\|4;1,0,m''\rangle$	$= \frac{1}{\sqrt{2}}\left[c^\dagger_{m\uparrow}c^\dagger_{m'\downarrow}+c^\dagger_{m\downarrow}c^\dagger_{m'\uparrow}\right]c^\dagger_{m''\uparrow}c^\dagger_{m''\downarrow}\|0\rangle$	$6U-13J$
$\|4;0,0,m''\rangle$	$= \frac{1}{\sqrt{2}}\left[c^\dagger_{m\uparrow}c^\dagger_{m'\downarrow}-c^\dagger_{m\downarrow}c^\dagger_{m'\uparrow}\right]c^\dagger_{m''\uparrow}c^\dagger_{m''\downarrow}\|0\rangle$	$6U-11J$
$\|4;0,0\rangle_a$	$= \frac{1}{\sqrt{3}}\left[c^\dagger_{xz\uparrow}c^\dagger_{xz\downarrow}c^\dagger_{yz\uparrow}c^\dagger_{yz\downarrow}+c^\dagger_{yz\uparrow}c^\dagger_{yz\downarrow}c^\dagger_{xy\uparrow}c^\dagger_{xy\downarrow}+c^\dagger_{xy\uparrow}c^\dagger_{xy\downarrow}c^\dagger_{xz\uparrow}c^\dagger_{xz\downarrow}\right]\|0\rangle$	$6U-8J$
$\|4;0,0\rangle_b$	$= \frac{1}{\sqrt{6}}\left[c^\dagger_{xz\uparrow}c^\dagger_{xz\downarrow}c^\dagger_{yz\uparrow}c^\dagger_{yz\downarrow}+c^\dagger_{yz\uparrow}c^\dagger_{yz\downarrow}c^\dagger_{xy\uparrow}c^\dagger_{xy\downarrow}-2c^\dagger_{xy\uparrow}c^\dagger_{xy\downarrow}c^\dagger_{xz\uparrow}c^\dagger_{xz\downarrow}\right]\|0\rangle$	$6U-11J$
$\|4;0,0\rangle_c$	$= \frac{1}{\sqrt{2}}\left[c^\dagger_{xz\uparrow}c^\dagger_{xz\downarrow}c^\dagger_{yz\uparrow}c^\dagger_{yz\downarrow}-c^\dagger_{yz\uparrow}c^\dagger_{yz\downarrow}c^\dagger_{xy\uparrow}c^\dagger_{xy\downarrow}\right]\|0\rangle$	$6U-11J$
$\|5;\frac{1}{2},\frac{\sigma}{2}\rangle$	$= c^\dagger_{m\sigma}c^\dagger_{m'\uparrow}c^\dagger_{m'\downarrow}c^\dagger_{m''\uparrow}c^\dagger_{m''\downarrow}\|0\rangle$	$10U-20J$
$\|6\rangle$	$= c^\dagger_{xz\uparrow}c^\dagger_{xz\downarrow}c^\dagger_{yz\uparrow}c^\dagger_{yz\downarrow}c^\dagger_{xy\uparrow}c^\dagger_{xy\downarrow}\|0\rangle$	$15U-30J$

Table 1: *The atomic t_{2g} states ($m = xy, xz, yz$) in the basis which diagonalize the Coulomb interaction. The label σ in the first column takes the value ± 1, while in the states it has the meaning $\uparrow$ or $\downarrow$. The labels m, m' and m'' indicate different orbitals.*

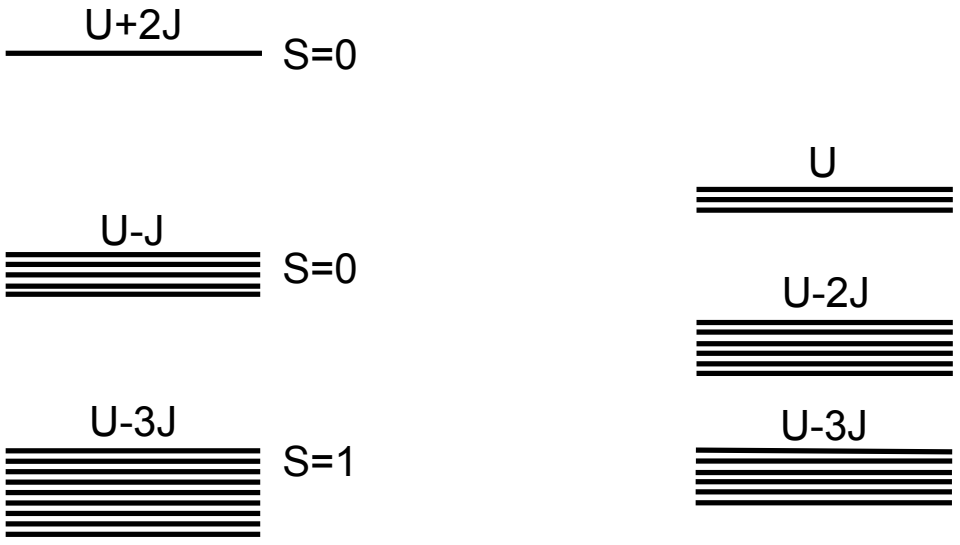

Fig. 10: *Atomic spectrum for the t_{2g}^2 configuration. Left: exact. Right: density-density approximation (spin-flip and pair-hopping terms set to zero). In the density-density approximation the total spin is not a good quantum number: The lower-energy block of states collects the $M_s = \pm 1$ states of the $S = 1$ triplet, and the middle block mixes $S = 0$ and $S = 1$ states. The average Coulomb interaction is $U - 2J$, both in the exact and the approximate case. The spectrum is identical for the t_{2g}^4 configuration, provided that all energies are shifted by $5U - 10J$.*

3.2 Low-symmetry crystal field, orbital order and orbital degeneracy

When the symmetry is lower that cubic, the t_{2g} levels can split. For example, if the symmetry is tetragonal, the t_{2g} states split into a doublet, xz, yz, and a singlet, xy; the tetragonal energy splitting is $\varepsilon_{\rm CF} = \varepsilon_{xy} - \varepsilon_{xz/yz}$. In metallic Sr_2RuO_4 the splitting $\varepsilon_{\rm CF}$ is relatively small (~ 120 eV), and the LDA+DMFT occupations of the different orbitals remain similar. In the insulating S-Pbca phase of Ca_2RuO_4, $\varepsilon_{\rm CF}$ is larger, ~ 300 meV, and the LDA+DMFT occupations are close to those of the $xy^2xz^1yz^1$ configuration (xy orbital-order). The Mott insulator $YTiO_3$ has even lower symmetry; because of the t_{2g}^1 configuration, only the lowest energy t_{2g} crystal-field level is actually occupied. Let us consider an oversimplified model for $YTiO_3$, i.e., a tetragonal system which, in the atomic limit, has configuration $xy^1xz^0yz^0$ at $T = 0$. How does the atomic Green-function matrix change with respect to the cubic case, Eq. (9)? The tetragonal symmetry implies that the imaginary time Green function has the matrix form

$$G^{\sigma}_{im,im'}(\tau) = \begin{pmatrix} G^{i\sigma}_{xy}(\tau) & 0 & 0 \\ 0 & G^{i\sigma}_{xz}(\tau) & 0 \\ 0 & 0 & G^{i\sigma}_{yz}(\tau) \end{pmatrix}, \quad \text{with} \quad G^{i\sigma}_{xz}(\tau) = G^{i\sigma}_{yz}(\tau).$$

For $k_BT \ll \varepsilon_{\rm CF} \ll U$, the xy Matsubara Green function is given by

$$G^{i\sigma}_{xy}(i\nu_n) \sim \frac{1}{6}\left(\frac{3}{i\nu_n + (\varepsilon_{xy} - \mu)} + \frac{2}{i\nu_n - (\varepsilon_{xy} + U - J - \mu)} + \frac{1}{i\nu_n - (\varepsilon_{xy} + U + 2J - \mu)}\right).$$

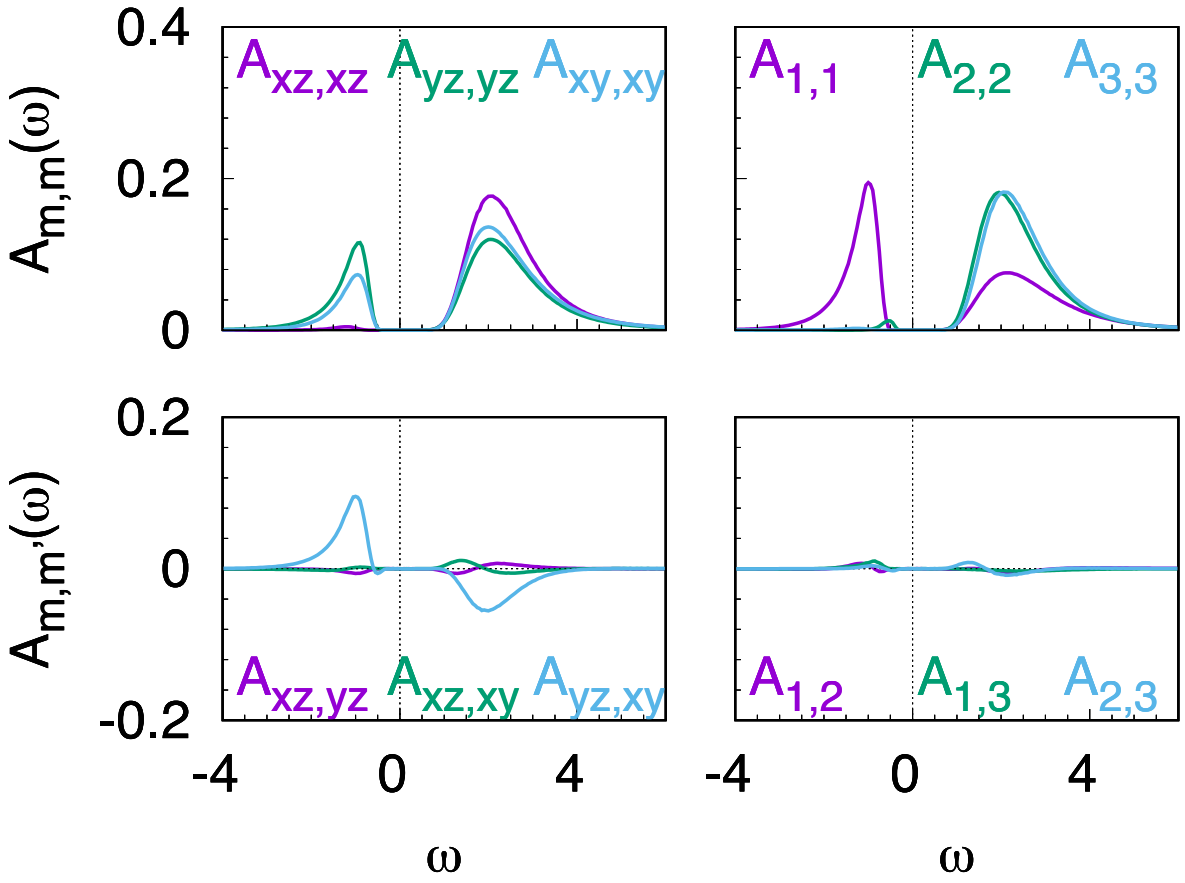

Fig. 11: *The LDA+DMFT spectral function matrix of the orbitally-ordered t_{2g}^1 system $YTiO_3$, in the (xz, yz, xy) basis (left panels) and in the crystal-field basis (right panels) [14, 17].*

Here we neglected the small mixing of the three high-energy $S = 0$ multiplets of the t_{2g}^2 configuration ($\varepsilon_{\rm CF} \ll U$). The xz and yz Matsubara Green functions take instead the form

$$G^{i\sigma}_{xz/yz}(i\nu_n) \sim \frac{1}{4}\left(\frac{3}{i\nu_n - (\varepsilon_{xz/yz} + U - 3J - \mu)} + \frac{1}{i\nu_n - (\varepsilon_{xz/yz} + U - J - \mu)}\right).$$

The atomic-limit gap is then

$$E_g(1) \sim U - 3J + \varepsilon_{\rm CF}.$$

From the expressions above we can see that the gap is inter-orbital and $\varepsilon_{\rm CF}$ increases it by a small amount. If the symmetry is lower than tetragonal, as in the case of $YTiO_3$, the Green function, the spectral-function and the self-energy become full 3×3 matrices. Still, in the atomic limit, a crystal-field splitting favors the occupation of the lowest energy t_{2g} crystal-field orbital. This remains true beyond the atomic limit: $YTiO_3$ is, indeed, an orbitally ordered Mott insulator with a gap of about 1 eV. This can be seen in the DMFT spectral-function matrix in Fig. 11. The crystal-field splitting not only increases the gap but also reduces orbital degeneracy, favoring the onset of a orbitally order Mott-insulating state. The importance of orbital degeneracy

for the Mott gap was explained for the first time by E. Koch, O. Gunnarsson and R.M. Martin [18, 19]. The argument presented in their works is the following. Let us assume that a system is described by the multi-orbital Hubbard model for t_{2g} electrons with, however, $J = 0$. Let us assume that, in addition, its ground state is antiferromagnetic, as it typically is. The states relevant for the gap are those generated by adding or removing one electron from the ground state. In the large-U limit their energy is approximately given by

$$\begin{aligned} E(N+1) &\sim nU + E(N) - \sqrt{k_+}\, W/2 \\ E(N-1) &\sim (n-1)U + E(N) - \sqrt{k_-}\, W/2, \end{aligned}$$

where n is the number of electrons per site and W is the band-width. The gap is then

$$E_g(N) \sim U - \frac{\sqrt{k}_- + \sqrt{k}_+}{2} W. \tag{10}$$

With respect to the atomic limit a term proportional to the bandwidth reduces the gap. To understand its origin we can go back to the case of the Hubbard dimer. For the dimer, the ground state is the singlet $|G\rangle_H$, given in Eq. (5). In the large-U limit

$$|G\rangle_H = |N\rangle \sim \frac{1}{\sqrt{2}} \left[c^\dagger_{1\uparrow} c^\dagger_{2\downarrow} - c^\dagger_{1\downarrow} c^\dagger_{2\uparrow} \right] |0\rangle.$$

By creating or removing an electron at site 1, we generate the states

$$\begin{aligned} c_{1\uparrow}|N\rangle &\sim \quad\quad + \frac{1}{\sqrt{2}}\, c^\dagger_{2\downarrow}|0\rangle = + \frac{1}{\sqrt{2}}\, |N-1\rangle_2 \\ c^\dagger_{1\uparrow}|N\rangle &\sim - \frac{1}{\sqrt{2}}\, c^\dagger_{1\uparrow} c^\dagger_{1\downarrow} c^\dagger_{2\uparrow}|0\rangle = - \frac{1}{\sqrt{2}}\, |N+1\rangle_2 \end{aligned}$$

By applying the non-interacting Hamiltonian, $\hat{H}_0$, we then have

$$\begin{aligned} \hat{H}_0|N-1\rangle_2 &= \quad\quad - t\, c^\dagger_{1\downarrow}|0\rangle = -t\, |N-1\rangle_1 \\ \hat{H}_0|N+1\rangle_2 &= + t\, c^\dagger_{2\uparrow} c^\dagger_{2\downarrow} c^\dagger_{1\uparrow}|0\rangle = +t\, |N+1\rangle_1 \end{aligned}$$

In the atomic limit, the states $\Big(|N-1\rangle_1, |N-1\rangle_2\Big)$ and the states $\Big(|N+1\rangle_1, |N+1\rangle_2\Big)$ are degenerate. For $t \neq 0$, in the spaces defined by each one of these couple of degenerate states, the Hamiltonian is

$$\hat{H}_{N_\pm} = \begin{pmatrix} E(N_\pm) & \pm t \\ \pm t & E(N_\pm) \end{pmatrix}$$

with $N_\pm = N \pm 1$. Thus the actual ground state is the bonding combination, and the associated bonding-energy gain is the square root of the second moment

$$M^{(2)}_\pm = {}_1\langle N_\pm | \hat{H}^2_0 | N_\pm \rangle_1 = t^2 = k_\pm (W/2)^2$$

where $W = 2t$ (energy difference between antibonding and bonding state), and $k_+ = k_- = 1$. The ground-state correction of atomic energies in first order degenerate perturbation theory is

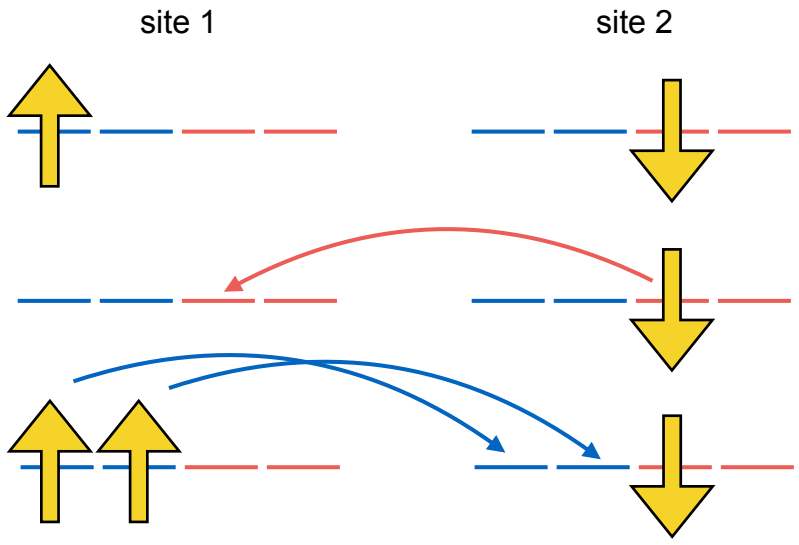

Fig. 12: *Possible hopping paths for an extra hole and an extra electron in the case of orbital degeneracy $d = 2$ and one electron per site. For simplicity only hopping between the same orbitals on neighboring sites is allowed. This figure was adapted from Fig. 4 of Ref. [19].*

thus $\Delta E(N_\pm) = -\sqrt{M_\pm^{(2)}}$. Indeed, as one can verify from the exact Green function given in section 2.1, in the large-U limit, the gap of the Hubbard dimer at half filling is $E_g(1) \sim U - 2t$. We can now generalize to the multi-orbital case. The second moment of the Hamiltonian is then $M_\pm^{(2)} = \langle N_\pm^i | \hat{H}_0^2 | N_\pm^i \rangle = \sum_j |\langle N_\pm^i | \hat{H}_0 | N_\pm^j \rangle|^2$, where $|N_\pm^i\rangle$ is the state generated by adding or removing from the ground state an electron at site i, and $|N_\pm^j\rangle$ are all the degenerate states generated from $|N_\pm^i\rangle$ by hopping. For the single orbital dimer, as we have seen, there is only one $|N_\pm^j\rangle$ state. If the number of degenerate orbitals d increases, however, so do the hopping possibilities; k_+ and k_- equal the number of available hopping paths, which depends of course on the actual model. Let us assume that $n = 1$ and $t_{m,m'}^{i,i'} = t_{m,m}^{\langle i,i' \rangle} \delta_{m,m'}$, i.e., only intra-orbital hopping between nearest neighbors is possible. If the model has two degenerate orbitals, $k_- = 1$. There are, however, two hopping possibilities for the extra electron, hence $k_+ = 2$. This is schematically illustrated in Fig. 12. As a result, in the orbitally-degenerate case there is a gap reduction with respect to the one-orbital case. This reduction, given in Eq. (10), can be viewed as a *hopping enhancement*. At half filling the enhancement factor is proportional to $\sqrt{d}$ [18,19]. The relevance of orbital degeneracy for the Mott gap and thus for the Mott transition became apparent in many cases. For example, orbital degeneracy can be reduced by a relatively small crystal-field splitting, as it was shown in Ref. [17] for the series of $3d^1$ perovskites. This happens because the crystal-field splitting makes some of the states higher in energy, so that they do not contribute to the second moment. Orbital degeneracy is also reduced by the Hund's rule coupling J, which makes some of the multiplets higher in energy, with similar effects. This effect plays a key role for Hund's metals [20].

3.3 Spin-orbit interaction

The main relativistic effect in solids is the spin-orbit interaction, whose strength grows increasing the atomic number Z. In correlated materials, the spin-orbit interaction competes with the Coulomb parameters, the crystal field, and the hopping integrals in determining magnetic and electronic properties. In the atomic limit, for the d shells the spin-orbit interaction is

$$\hat{H}_{\rm SO} = \sum_{\mu} \lambda_{\mu} \sum_{mm'} \sum_{\sigma\sigma'} \epsilon^{\mu}_{m\sigma,m'\sigma'}\, c^{\dagger}_{m\sigma} c_{m'\sigma'}, \qquad \epsilon^{\mu}_{m\sigma,m'\sigma'} = \langle m\sigma | l_{\mu} s_{\mu} | m'\sigma' \rangle,$$

where $\mu = x, y, z$, and λ_{μ} are the spin-orbit couplings, with $\lambda_{\mu} = \lambda$ in $O(3)$ symmetry, and

$$\lambda \sim g\mu_B^2 \left\langle \frac{1}{r} \frac{d}{dr} v_R(r) \right\rangle .$$

Let us assume that, according to the first and second of Hund's rules, S is the total spin and L the total angular momentum of the ground multiplet; these LS states are $(2L+1)(2S+1)$-fold degenerate. If the spin-orbit coupling λ is small compared to the Hund's rule couplings J_1 and J_2, the spin-orbit interaction can be treated as a perturbation splitting the LS manifold in eigenstates of the total angular momentum j. The third Hund's rule states that, if the outermost shell is less than half filled, the ground multiplet is the one with $j = L - S$; if, instead, it is more than half filled, it is the one with $j = L + S$. For the d^1 configuration, $L = 2$ and $S = 1/2$, so that the quartet $j = 3/2$ is the ground multiplet. In materials, the second and third of Hund's rules, and sometimes, as we have discussed, even the first, can be violated. This happens also in Mott insulators, where the atomic character is preserved to a large extent. A source of Hund's rules breakdown is the crystal field. The strength of the spin-orbit interaction λ has therefore to be compared not only to J_1 and J_2 but also to the relevant crystal-field couplings. In that respect, it is important to notice that $\hat{H}_{\rm SO}$ couples e_g and t_{2g} states. If, however, the cubic crystal field $\varepsilon_{\rm C}$ is large compared to λ, as typically is the case for $4d$ systems, and the electronic configuration without spin-orbit interaction is $t_{2g}^n e_g^0$, we can safely downfold the e_g states. For cubic t_{2g} systems of this kind, the spin-orbit Hamiltonian can then be rewritten as

$$\begin{aligned} \hat{H}_{\rm SO} = & \frac{i\lambda}{2} \left(\sum_{\sigma} \sigma \; c^{\dagger}_{yz\sigma} c_{xz\sigma} + c^{\dagger}_{xz\uparrow} c_{xy\downarrow} + i c^{\dagger}_{yz\uparrow} c_{xy\downarrow} + c^{\dagger}_{xz\downarrow} c_{xy\uparrow} - i c^{\dagger}_{yz\downarrow} c_{xy\uparrow} \right) + \text{h.c.} \\ = & -\frac{\lambda}{2} \left[\sum_{\sigma m} m\sigma c^{\dagger}_{m\sigma} c_{m\sigma} + \sqrt{2} \left(c^{\dagger}_{-1\uparrow} c_{0\downarrow} + c^{\dagger}_{0\uparrow} c_{+1\downarrow} + c^{\dagger}_{+1\downarrow} c_{0\uparrow} + c^{\dagger}_{0\downarrow} c_{-1\uparrow} \right) \right], \end{aligned} \tag{11}$$

where

$$c^{\dagger}_{-1,\sigma} = -\frac{c^{\dagger}_{xz,\sigma} + i c^{\dagger}_{yz,\sigma}}{\sqrt{2}}, \qquad c^{\dagger}_{+1,\sigma} = -\frac{c^{\dagger}_{xz,\sigma} - i c^{\dagger}_{yz,\sigma}}{\sqrt{2}}, \qquad c^{\dagger}_{0,\downarrow} = -i c^{\dagger}_{xy,\sigma}.$$

In the last line of Eq. (11) we have brought the spin-orbit interaction in the form it takes for p electrons (effective angular momentum $l = 1$), apart, however, a minus sign in front. For the t_{2g}^1 configuration the effective total angular momentum j can thus have the values $3/2$ and $1/2$. The

local Green function matrix reflects the presence of spin-orbit interaction via extra off-diagonal terms. For a t_{2g} system with cubic symmetry its most general form is [21, 23]

$$G^{\sigma,\sigma'}_{im,im'}(\tau) = \left(\begin{array}{ccc|ccc} G^{i\uparrow\uparrow}_{xy}(\tau) & 0 & 0 & 0 & G^{i\uparrow\downarrow}_{y}(\tau) & -iG^{i\uparrow\downarrow}_{x}(\tau) \\ 0 & G^{i\uparrow\uparrow}_{yz}(\tau) & iG^{i\uparrow\uparrow}_{z}(\tau) & -G^{i\uparrow\downarrow}_{y}(\tau) & 0 & 0 \\ 0 & -iG^{i\uparrow\uparrow}_{z}(\tau) & G^{i\uparrow\uparrow}_{xz}(\tau) & iG^{i\uparrow\downarrow}_{x}(\tau) & 0 & 0 \\ \hline 0 & -G^{i\downarrow\uparrow}_{y}(\tau) & -iG^{i\downarrow\uparrow}_{x}(\tau) & G^{i\downarrow\downarrow}_{xy}(\tau) & 0 & 0 \\ G^{i\downarrow\uparrow}_{y}(\tau) & 0 & 0 & 0 & G^{i\downarrow\downarrow}_{yz}(\tau) & -iG^{i\downarrow\downarrow}_{z}(\tau) \\ iG^{i\downarrow\uparrow}_{x}(\tau) & 0 & 0 & 0 & iG^{i\uparrow\uparrow}_{z}(\tau) & G^{i\downarrow\downarrow}_{xz}(\tau) \end{array}\right)$$

where all $G^{i\sigma\sigma'}_{m}(\tau)$ are real functions, and $G^{i\sigma\sigma'}_{m}(\tau) = G^{i\sigma'\sigma}_{m}(\tau)$, while $G^{i\sigma\sigma'}_{x}(\tau) = G^{i\sigma\sigma'}_{y}(\tau) = G^{i\sigma\sigma'}_{z}(\tau)$, and $G^{i\sigma\sigma}_{xz}(\tau) = G^{i\sigma\sigma}_{yz}(\tau) = G^{i\sigma\sigma}_{xy}(\tau)$. The local Green function above is diagonal in the basis of the eigenstates of the total angular momentum of the t^1_{2g} configuration. Among those, the $j = 3/2$ quartet is generated by the creation operators

$$c^\dagger_{-\frac{3}{2}} = c^\dagger_{-1,\downarrow} \qquad c^\dagger_{-\frac{1}{2}} = \frac{c^\dagger_{-1,\uparrow} + \sqrt{2}c^\dagger_{0,\downarrow}}{\sqrt{3}} \qquad c^\dagger_{+\frac{1}{2}} = \frac{c^\dagger_{+1,\downarrow} + \sqrt{2}c^\dagger_{0,\uparrow}}{\sqrt{3}}, \qquad c^\dagger_{+\frac{3}{2}} = c^\dagger_{+1,\uparrow}.$$

Instead, the $j = 1/2$ doublet is generated by the creation operators

$$d^\dagger_{-\frac{1}{2}} = -\frac{\sqrt{2}c^\dagger_{-1,\uparrow} - c^\dagger_{0,\downarrow}}{\sqrt{3}} \qquad d^\dagger_{+\frac{1}{2}} = \frac{\sqrt{2}c^\dagger_{+1,\downarrow} - c^\dagger_{0,\uparrow}}{\sqrt{3}}.$$

By inverting these relations, we can express the t_{2g} creation and destruction operators as

$$c^\dagger_{xz,\downarrow} = \frac{1}{\sqrt{6}}\left[-\sqrt{3}c^\dagger_{-\frac{3}{2}} - c^\dagger_{\frac{1}{2}} - \sqrt{2}d^\dagger_{\frac{1}{2}}\right] \qquad c^\dagger_{xz,\uparrow} = \frac{1}{\sqrt{6}}\left[-\sqrt{3}c^\dagger_{\frac{3}{2}} - c^\dagger_{-\frac{1}{2}} + \sqrt{2}d^\dagger_{-\frac{1}{2}}\right]$$

$$c^\dagger_{yz,\downarrow} = \frac{i}{\sqrt{6}}\left[+\sqrt{3}c^\dagger_{-\frac{3}{2}} - c^\dagger_{\frac{1}{2}} - \sqrt{2}d^\dagger_{\frac{1}{2}}\right] \qquad c^\dagger_{yz,\uparrow} = \frac{i}{\sqrt{6}}\left[-\sqrt{3}c^\dagger_{\frac{3}{2}} + c^\dagger_{-\frac{1}{2}} - \sqrt{2}d^\dagger_{-\frac{1}{2}}\right]$$

$$c^\dagger_{xy,\downarrow} = \frac{i}{\sqrt{3}}\left[+\sqrt{2}c^\dagger_{-\frac{1}{2}} + d^\dagger_{-\frac{1}{2}}\right] \qquad c^\dagger_{xy,\uparrow} = \frac{i}{\sqrt{3}}\left[+\sqrt{2}c^\dagger_{\frac{1}{2}} - d^\dagger_{\frac{1}{2}}\right],$$

and rewrite the Green function matrix in the new basis. It takes the simple form

$$G^{j,j'}_{im_j,im_{j'}}(\tau) = G^{i\uparrow\uparrow}_{\frac{3}{2}}(\tau)\hat{I}_{\frac{3}{2}} + G^{i\uparrow\uparrow}_{\frac{1}{2}}(\tau)\hat{I}_{\frac{1}{2}},$$

where $\hat{I}_j$ is the identity matrix of dimension $2j + 1$. The spin-orbit Hamiltonian has the same diagonal form

$$\hat{H}_{\rm SO} = -\frac{\lambda}{2}\sum_{m=-\frac{3}{2}}^{+\frac{3}{2}} \hat{n}_{\frac{3}{2},m} + \lambda \sum_{m=-\frac{1}{2}}^{+\frac{1}{2}} \hat{n}_{\frac{1}{2},m}.$$

One could thus conclude that the total angular momentum basis is the ideal one in the presence of spin-orbit interaction. We have, however, to pay attention to the fact that the crystal-field Hamiltonian is not diagonal in the angular momentum basis. Furthermore, if we change basis in the way just described, we have to transform accordingly $\hat{H}_U$, the Coulomb part of the Hamiltonian. We can see some of the effects of this transformation by considering a tetragonal system for which $\varepsilon_{\rm CF}$, the tetragonal crystal-field splitting, is very large. In such a case the xy orbital is basically decoupled and we can assume $\hat{H}_{\rm SO} \sim \hat{H}^z_{\rm SO} = \frac{i\lambda_z}{2} \sum_\sigma \sigma \; c^\dagger_{yz\sigma} c_{xz\sigma}$. The interaction $\hat{H}^z_{\rm SO}$ is diagonal in the basis of spherical harmonics. The corresponding creation operators are

$$c^\dagger_{-\frac{3}{2}} = c^\dagger_{-1,\downarrow} \qquad c^\dagger_{-\frac{1}{2}} = c^\dagger_{-1,\uparrow} \qquad c^\dagger_{+\frac{3}{2}} = c^\dagger_{+1,\uparrow} \qquad c^\dagger_{+\frac{1}{2}} = c^\dagger_{+1,\downarrow}.$$

In the spherical harmonics basis the Coulomb interaction for xz/yz orbitals takes the form

$$\begin{aligned}\hat{H}_U =& (U-J)\big(\hat{n}_{\frac{3}{2}}\hat{n}_{\frac{1}{2}} + \hat{n}_{-\frac{3}{2}}\hat{n}_{-\frac{1}{2}} + \hat{n}_{\frac{3}{2}}\hat{n}_{-\frac{3}{2}} + \hat{n}_{\frac{1}{2}}\hat{n}_{-\frac{1}{2}}\big) \\ &+ (U-3J)\big(\hat{n}_{\frac{3}{2}}\hat{n}_{-\frac{1}{2}} + \hat{n}_{-\frac{3}{2}}\hat{n}_{\frac{1}{2}}\big) \; - 2J\big(c^\dagger_{\frac{3}{2}} c_{\frac{1}{2}} c^\dagger_{-\frac{3}{2}} c_{-\frac{1}{2}} + c^\dagger_{-\frac{1}{2}} c_{-\frac{3}{2}} c^\dagger_{\frac{1}{2}} c_{\frac{3}{2}}\big).\end{aligned}$$

Thus, we can see that in the new basis the pair-hopping terms are zero and the density-density terms have a different prefactor than in the original xz, yz basis.[9]

What about LDA+DMFT calculations with spin-orbit interaction? Although $\hat{H}_{\rm SO}$ looks like an innocent one-body term, it turns out that, for real materials, calculations including this term are more difficult. This has two reasons: (i) they involve larger Green function matrices, e.g., 6×6 as in the case just discussed, hence they are more demanding computationally and (ii) they are often hampered by a much stronger sign problem. Thus, specific basis choices and approximations are used. A possible approach consists in working in the basis that diagonalizes the non-interacting local Green function or the non-interacting local Hamiltonian; such a basis typically reduces the sign problem, as was first shown in Ref. [10] for the case without spin-orbit interaction. For a system with tetragonal symmetry, the states that diagonalize the local Green function belong either to the Γ_6 or to the Γ_7 irreducible representations, both 2-dimensional. There are two (coulped) Γ_7 representations, defining the space $\Gamma_7' \oplus \Gamma_7''$. The analytic expression of these states can be found in Refs. [16, 21, 23]. The transformation to the $\Gamma_6 \oplus \Gamma_7' \oplus \Gamma_7''$ basis is, of course, in principle, a mere basis change. Approximations are made, however, if all off-diagonal elements of the Green function are set to zero or the Coulomb tensor is truncated, as often done, e.g., to further tame the sign problem.

In the presence of crystal-field splitting, if the spin-orbit interaction does not dominate, it is often preferable to perform the calculations in the t_{2g} basis. To this end, it is key to make QMC codes very efficient in order to reduce as much as possible statistical errors and increase the average sign. Exact LDA+SO+DMFT calculations in the t_{2g} basis have been successfully performed for Sr_2RuO_4, using an interaction-expansion continuous-time quantum Monte Carlo solver, and an orbital-dependent phase which makes the Green function matrix real [21, 23].

[9] For the transformation of the full Coulomb tensor from cubic to spherical harmonics, see, e.g., my chapter in Ref. [12]. It goes without saying that the total Green function (hence the gap) and the energy of the multiplets do not change if we change basis, although the components of the Green functions are basis dependent.

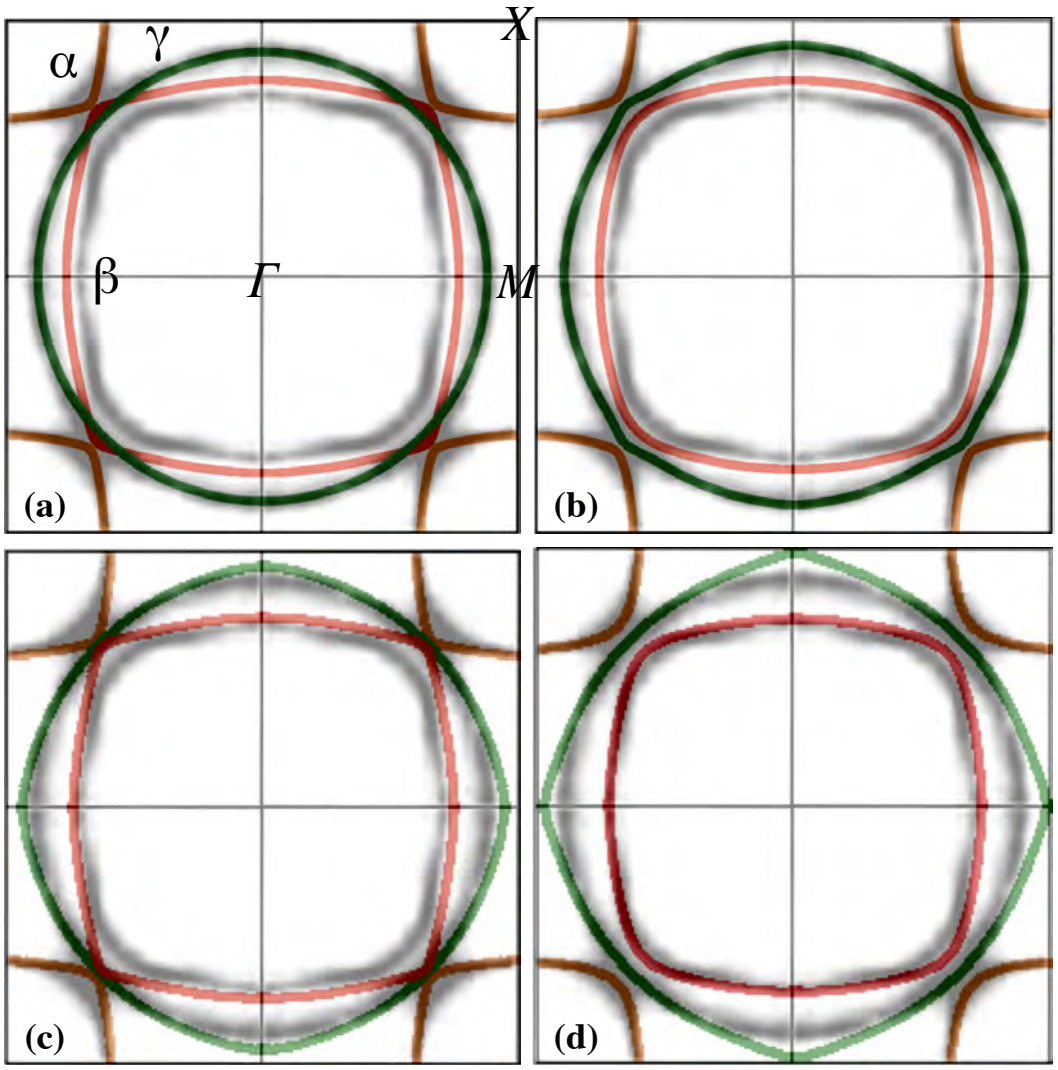

Fig. 13: *Fermi surface of Sr_2RuO_4 calculated with LDA (a), LDA+SO (b), LDA+DMFT (c) and LDA+SO+DMFT (d) [21]. The grey maps are experimental results from Ref. [22].*

This approach allowed us to study, for example, the effects of the spin-orbit interaction on the Fermi surface without approximations. The results are shown in Fig. 13 in comparison with experimental data; we will discuss them in the next section. In Fig. 14 we show instead another example of LDA+SO+DMFT calculations, the orbital-resolved spectral function matrix of Ca_2RuO_4. The figure compares the spectral function matrices for the metallic L-Pbca phase and the insulating S-Pbca phase, both with and without spin-orbit interaction. In the case of the S-Pbca phase, the spectral function matrix shows that the system is orbitally ordered, with the configuration $\sim xy^2\, xz^1\, yz^1$ corresponding to xy orbital order. The small gap is inter-orbital, and more specifically $xy \to xz, yz$.

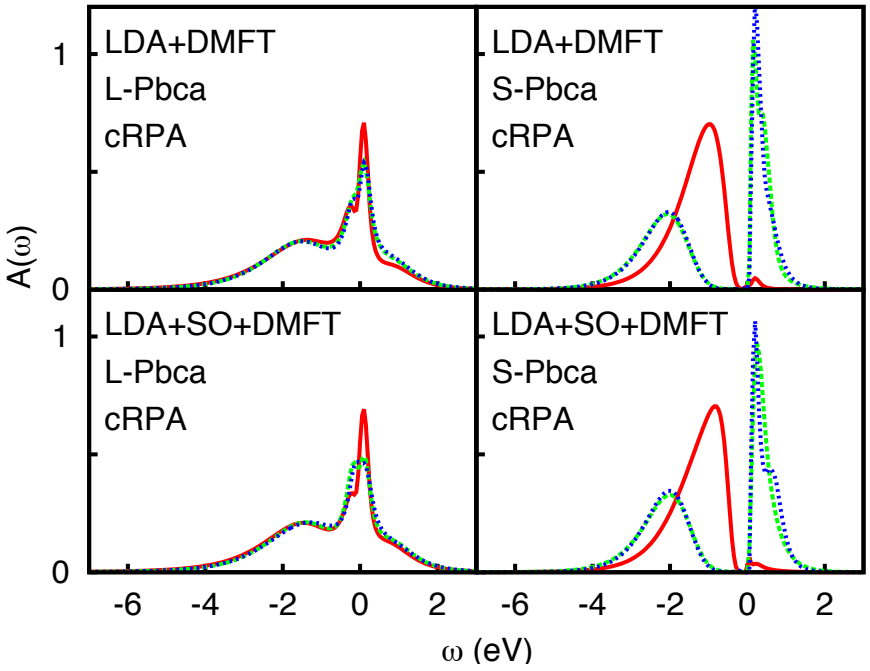

Fig. 14: *Spectral function matrix for the t_{2g}^4 system Ca_2RuO_4. Left: high-temperature L-Pbca metallic phase. Right: Low-temperature insulating S-Pbca phase.*

3.4 Non-spherical Coulomb terms and double-counting correction

Up to now we have considered the Coulomb tensor spherical (symmetry $O(3)$). This is exact for a free atom. The screened Coulomb tensor has, however, in general, the symmetry of the lattice. Taking into account non-spherical Coulomb terms is, in general hard, both because they make QMC calculations more difficult and can worsen the sign problem, and because in their presence the double-counting correction has to be explicitly accounted for, even when massive downfolding is used. For these reasons they are typically neglected. Recently it was shown that they can play a very important role for the Fermi surface, however [21]. Let us therefore discuss how the double-counting correction can be treated in the presence of such terms, following the approach of Ref. [21]. One of the classical approximations for the double-counting correction is the so called "around mean-field" approximation. The idea is that LDA describes well the average Coulomb term, in the absence of orbital polarization. This is equivalent to using as double-counting correction the Hartree term of the Coulomb interaction tensor, i.e., the operator

$$\begin{aligned}\hat{H}_{\mathrm{U}}^{\mathrm{DC}} &= U\sum_{m}\left(\hat{n}_{m\uparrow}\bar{n}_{m\downarrow}+\bar{n}_{m\uparrow}\hat{n}_{m\downarrow}\right)+(U-2J)\sum_{m\neq m'}\left(\hat{n}_{m\uparrow}\bar{n}_{m'\downarrow}+\bar{n}_{m\uparrow}\hat{n}_{m'\downarrow}\right)\\ &+(U-3J)\sum_{\sigma}\sum_{m>m'}\left(\hat{n}_{m\sigma}\bar{n}_{m'\sigma}+\bar{n}_{m\sigma}\hat{n}_{m'\sigma}\right)-\mu\hat{N}_d\\ &-U\sum_{m}\bar{n}_{m\uparrow}\bar{n}_{m\downarrow}+(U-2J)\sum_{m\neq m'}\bar{n}_{m\uparrow}\bar{n}_{m'\downarrow}+(U-3J)\sum_{\sigma}\sum_{m>m'}\bar{n}_{m\sigma}\bar{n}_{m'\sigma}\end{aligned}$$

where $\bar{n}_{m\sigma} = n/d$, if n is the number of the correlated electrons per site and d the orbital degeneracy. Within this approximation we have, after collecting all terms,

$$\begin{aligned}\hat{H}_{\rm U}^{\rm DC} =&(\delta\mu - \mu)\hat{N}_d - \frac{n^2}{d}\left[U\,(2d-1) - 5\,(d-1)\,\right]\\ \delta\mu =&\frac{n}{d}\big[U(2d-1) - 5J(d-1)\big].\end{aligned}$$

If we perform massive downfolding to the correlated bands, as previously mentioned, this is merely a shift of the chemical potential and can therefore be neglected. Let us now consider the case in which the Coulomb interaction has an additional term that does not change the average U but has tetragonal symmetry

$$\Delta\hat{H}_U = \frac{\Delta U}{3}\Big(2\hat{n}_{xy\uparrow}\hat{n}_{xy\downarrow} - \hat{n}_{xz\uparrow}\hat{n}_{xz\downarrow} - \hat{n}_{yz\uparrow}\hat{n}_{yz\downarrow}\Big)$$

We can now use the around mean-field approximation for this term as well. We find

$$\begin{aligned}\Delta\hat{H}_U^{\rm DC} &= \frac{n}{6}\frac{\Delta U}{3}\sum_\sigma\Big(2\hat{n}_{xy\sigma} - \hat{n}_{xz\sigma} - \hat{n}_{yz\sigma}\Big) = \frac{n}{6}\Delta U\sum_\sigma \hat{n}_{xy\sigma} - \delta\mu'\hat{N}\\ \delta\mu' &= \frac{n}{6}\frac{\Delta U}{3}.\end{aligned}$$

This term, in addition to a shift of the chemical potential, yields an effective change of the crystal-field splitting $\varepsilon_{\rm CF}$, and has therefore to be accounted for explicitly.

How does ΔU changes the Fermi surface of Sr_2RuO_4? The Fermi surface is determined by the poles of the Green function at zero frequency. These depend on the non-interacting Hamiltonian and the self-energy matrix at zero frequency. In the Fermi-liquid regime, and within the DMFT local approximation, the effect of the self-energy is merely to modify the on-site part of the Hamiltonian, i.e., the crystal-field splitting and the spin-orbit couplings

$$\varepsilon_{\rm CF} \to \varepsilon_{\rm CF} + \Delta\varepsilon_{\rm CF}(0),$$

$$\lambda_\mu \to \lambda_\mu + \Delta\lambda_\mu(0).$$

Both $\Delta\varepsilon_{\rm CF}(0)$ and $\Delta\lambda_\mu(0)$ are positive for Sr_2RuO_4, and lead to an almost doubling of the LDA parameters. The positive $\Delta\varepsilon_{\rm CF}(0)$ shrinks the β sheet (xz/yz bands) and enlarges the γ (xy band) sheet. This can be understood from the schematic Fermi surface and the LDA band structure in Fig. 9. Enhancing the crystal-field splitting corresponds to slightly moving the xy band downwards and the xz/yz bands upwards with respect to the Fermi level. The enhancement of the spin-orbit couplings has a large Hartree-Fock component [23], since the spin-orbit interaction yields a small but finite off-diagonal occupation matrix. For a $O(3)$-symmetric Coulomb tensor, the Hartree-Fock enhancement of the spin-orbit coupling is thus

$$\begin{aligned}\frac{\Delta\lambda_z}{2} &= \quad i(U-3J)\,n^{\uparrow\uparrow}_{xz,yz}\\ \frac{\Delta\lambda_y}{2} &= -\,(U-3J)\,n^{\uparrow\downarrow}_{xy,yz},\\ \frac{\Delta\lambda_x}{2} &= -i(U-3J)\,n^{\uparrow\downarrow}_{xy,xz},\end{aligned}$$

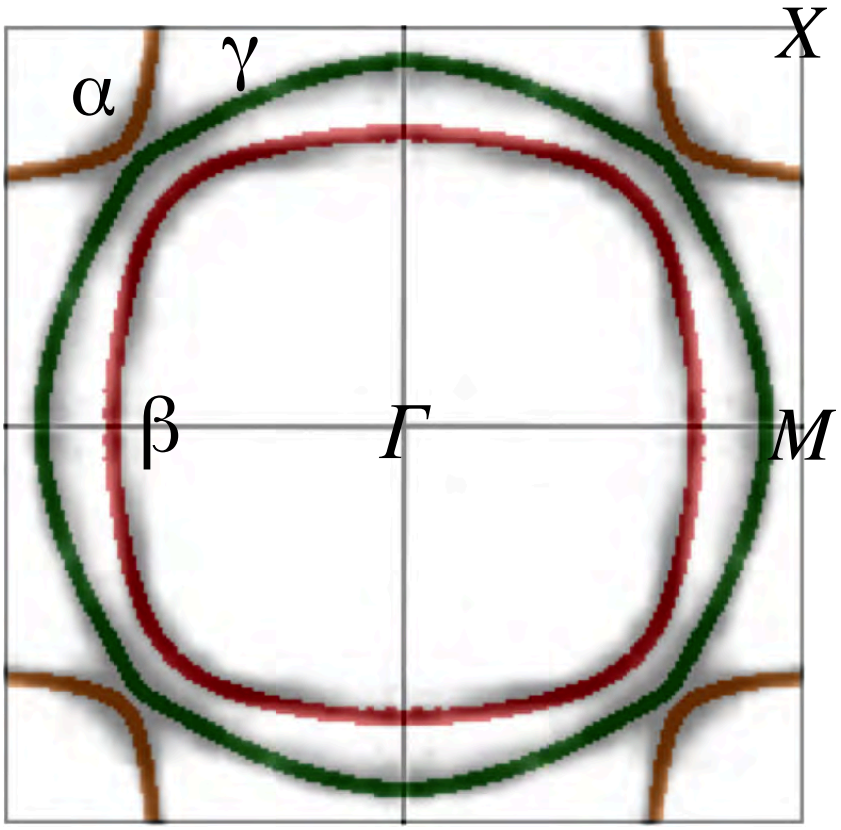

Fig. 15: *The LDA+SO+DMFT Fermi surface of Sr_2RuO_4 calculated including the effects of the non-spherical Coulomb term ΔU.*

where $n^{\sigma\sigma'}_{m,m'}$ are the off-diagonal elements of the density matrix. The Coulomb-enhanced spin-orbit coupling improves the agreement with the experimental Fermi surface at the degeneracy points (e.g., along the Γ-X direction). The agreement with ARPES data, however, further deteriorates for the γ sheet. This can be seen in Fig. 13, in which the LDA and LDA+DMFT Fermi surface are shown on top of ARPES data from Ref. [22].

Including correlation effects has thus two opposite effects: on the one hand, the agreement with experiments improves with respect to LDA for the β sheet; on the other hand, it deteriorates for the γ sheet. This can be seen comparing either panels (a) and (c) or panels (b) and (d) in Fig. 13. Introducing tetragonal terms, and in particular the term ΔU, however, reduces the crystal-field enhancement to

$$\varepsilon_{\rm CF} \rightarrow \varepsilon_{\rm CF} + \Delta\varepsilon'_{\rm CF}(0),$$

where $\Delta\varepsilon'_{\rm CF}(0)$ becomes almost zero for cRPA-based estimates of ΔU. This leads to an almost perfect Fermi surface, as shown in Fig. 15. Non-spherical Coulomb terms turn out to be more important for properties that reflect the point symmetry of the lattice, like the Fermi surface, than for properties that average over orbitals, like total spectral function [23].

4 Conclusion

The many-body problem is the grand challenge of solid-state physics. The result of many electrons interacting together is a plethora of co-operative emergent properties. Among these are heavy quasiparticles and the Coulomb-driven metal-insulator transition. The LDA+DMFT approach has opened the possibility of describing and understanding these phenomena in real materials. This approach is based on the DMFT local approximation for the self-energy. DMFT is exact in several limits: the non-interacting limit, the atomic limit, and the limit of infinite coordination number. In typical strongly-correlated materials it turns out to be an excellent approximation. Approaches that go beyond the local approximation range from cluster extensions to various diagrammatic methods, among which the dual-particle based techniques. A key aspect of DMFT remains model building. Essential to that is the basis choice. The basis should be as localized as possible but should also carry as much information as possible about the actual system. Crucial is to chose a basis which indeed spans the whole space of correlated electrons, even if this reduces localization. Wannier functions built from LDA/GGA calculations satisfy all these requirements. It is also important to take into account the symmetry of the system, and consider the effect of small distortions – unless including them makes calculations impossible. We have seen in many cases that small details do matter. A small crystal-field can favor the onset of the metal-insulator transition [17]. Small non-spherical Coulomb terms can sizably deform the Fermi surface of a multi-band correlated metal [21]. Improving the models and developing new methods to solve complex realistic models is therefore key for future progress. While numerical codes become always more sophisticated, many-body physics is primarily driven by experimental discoveries, novel phenomena whose interpretation remain often a mystery for decades. Indeed, one can identify only very few cases in which theory has predicted unknown emergent phenomena. A famous example is anti-ferromagnetism, which was predicted using static mean-field theory. Remarkably, it turned out later that the original theoretical description was wrong. In the future there will be new classes of supercomputers and algorithms which will allow us to run always more realistic simulations. Although prediction will remain difficult, our ability of reconstructing experimental results will steadily increase. As physicists, however, our role is to understand and explain phenomena, not merely reproduce them. Even a calculation that reproduce exactly experiments does not add new knowledge, if it does not help us in explaining the origin of the observed phenomenon. This would be like having the exact solution of the classical N-body problem discussed in the introduction, from which we are not able to learn anything. Our major task remains thus to identify, with the help of computers and algorithms, the mechanisms behind phenomena, building a coherent picture.

Appendices

A The Anderson molecule

The Hamiltonian of the Anderson molecule is given by

$$\hat{H} = \varepsilon_s \sum_\sigma \hat{n}_{2\sigma} - t \sum_\sigma \left(c^\dagger_{1\sigma} c_{2\sigma} + c^\dagger_{2\sigma} c_{1\sigma} \right) + \varepsilon_d \sum_\sigma \hat{n}_{1\sigma} + U \hat{n}_{1\uparrow} \hat{n}_{1\downarrow}.$$

It commutes with the number of electron operator $\hat{N}$, with the total spin $\hat{S}$ and with $\hat{S}_z$. Thus we can express the many-body states in the atomic limit as

$\lvert N, S, S_z \rangle$			N	S	$E(N,S)$
$\lvert 0,0,0 \rangle$	$=$	$\lvert 0 \rangle$	0	0	0
$\lvert 1,1/2,\sigma \rangle_1$	$=$	$c^\dagger_{1\sigma} \lvert 0 \rangle$	1	$1/2$	ε_d
$\lvert 1,1/2,\sigma \rangle_2$	$=$	$c^\dagger_{2\sigma} \lvert 0 \rangle$	1	$1/2$	ε_s
$\lvert 2,1,0 \rangle$	$=$	$\frac{1}{\sqrt{2}} \left[c^\dagger_{1\uparrow} c^\dagger_{2\downarrow} + c^\dagger_{1\downarrow} c^\dagger_{2\uparrow} \right] \lvert 0 \rangle$	2	1	$\varepsilon_d + \varepsilon_s$
$\lvert 2,1,1 \rangle$	$=$	$c^\dagger_{2\uparrow} c^\dagger_{1\uparrow} \lvert 0 \rangle$	2	1	$\varepsilon_d + \varepsilon_s$
$\lvert 2,1,-1 \rangle$	$=$	$c^\dagger_{2\downarrow} c^\dagger_{1\downarrow} \lvert 0 \rangle$	2	1	$\varepsilon_d + \varepsilon_s$
$\lvert 2,0,0 \rangle_0$	$=$	$\frac{1}{\sqrt{2}} \left[c^\dagger_{1\uparrow} c^\dagger_{2\downarrow} - c^\dagger_{1\downarrow} c^\dagger_{2\uparrow} \right] \lvert 0 \rangle$	2	0	$\varepsilon_d + \varepsilon_s$
$\lvert 2,0,0 \rangle_1$	$=$	$c^\dagger_{1\uparrow} c^\dagger_{1\downarrow} \lvert 0 \rangle$	2	0	$2\varepsilon_d + U$
$\lvert 2,0,0 \rangle_2$	$=$	$c^\dagger_{2\uparrow} c^\dagger_{2\downarrow} \lvert 0 \rangle$	2	0	$2\varepsilon_s$
$\lvert 3,1/2,\sigma \rangle_1$	$=$	$c^\dagger_{1\sigma} c^\dagger_{2\uparrow} c^\dagger_{2\downarrow} \lvert 0 \rangle$	3	$1/2$	$\varepsilon_d + 2\varepsilon_s$
$\lvert 3,1/2,\sigma \rangle_2$	$=$	$c^\dagger_{2\sigma} c^\dagger_{1\uparrow} c^\dagger_{1\downarrow} \lvert 0 \rangle$	3	$1/2$	$2\varepsilon_d + \varepsilon_s + U$
$\lvert 4,0,0 \rangle$	$=$	$c^\dagger_{1\uparrow} c^\dagger_{1\downarrow} c^\dagger_{2\uparrow} c^\dagger_{2\downarrow} \lvert 0 \rangle$	4	0	$2\varepsilon_d + 2\varepsilon_s + U$

For $N = 1$ electrons the Hamiltonian can be written in the matrix form

$$\hat{H}_1 = \begin{pmatrix} \varepsilon_d & -t & 0 & 0 \\ -t & \varepsilon_s & 0 & 0 \\ 0 & 0 & \varepsilon_d & -t \\ 0 & 0 & -t & \varepsilon_s \end{pmatrix}.$$

The eigenstates are thus

$\lvert 1,S,S_z \rangle_\alpha$	$E_\alpha(1,S)$	$d_\alpha(1,S)$
$\lvert 1,1/2,\sigma \rangle_+ = \alpha_1 \lvert 1,1/2,\sigma \rangle_1 - \alpha_2 \lvert 1,1/2,\sigma \rangle_2$	$\frac{1}{2}\left[\varepsilon_d + \varepsilon_s + \sqrt{(\varepsilon_d - \varepsilon_s)^2 + 4t^2} \right]$	2
$\lvert 1,1/2,\sigma \rangle_- = \alpha_2 \lvert 1,1/2,\sigma \rangle_1 + \alpha_1 \lvert 1,1/2,\sigma \rangle_2$	$\frac{1}{2}\left[\varepsilon_d + \varepsilon_s - \sqrt{(\varepsilon_d - \varepsilon_s)^2 + 4t^2} \right]$	2

where $d_\alpha(N)$ is the spin degeneracy of the α manifold. For $\varepsilon_s = \varepsilon_d + U/2$ the eigenvalues are

$$E_\pm(1,S) = \varepsilon_d + \frac{1}{4}\big[U \pm \Delta(U,t)\big],$$

where

$$\Delta(t,U) = \sqrt{U^2 + 16t^2}.$$

The parameters α_1 and α_2 of the corresponding eigenvectors are

$$\alpha_1^2 = \frac{1}{\Delta(t,U)}\frac{\Delta(t,U)-U}{2} \qquad\qquad \alpha_2^2 = \frac{4t^2}{\Delta(t,U)}\frac{2}{\Delta(t,U)-U}$$

For N=2 electrons, the hopping integrals only couple the S=0 states. The Hamiltonian is

$$\hat{H}_2 = \begin{pmatrix} \varepsilon_d{+}\varepsilon_s & 0 & 0 & 0 & 0 & 0 \\ 0 & \varepsilon_d{+}\varepsilon_s & 0 & 0 & 0 & 0 \\ 0 & 0 & \varepsilon_d{+}\varepsilon_s & 0 & 0 & 0 \\ 0 & 0 & 0 & \varepsilon_d{+}\varepsilon_s & -\sqrt{2}t & -\sqrt{2}t \\ 0 & 0 & 0 & -\sqrt{2}t & 2\varepsilon_d{+}U & 0 \\ 0 & 0 & 0 & -\sqrt{2}t & 0 & 2\varepsilon_s \end{pmatrix}$$

For $\varepsilon_s = \varepsilon_d + U/2$ the eigenvalues and the corresponding eigenvectors are

$\|2,S,S_z\rangle_\alpha$	$E_\alpha(2,S)$	$d_\alpha(2,S)$
$\|2,0,0\rangle_+ = a_1\|2,0,0\rangle_0 - \frac{a_2}{\sqrt{2}}\left[\|2,0,0\rangle_1 + \|2,0,0\rangle_2\right]$	$2\varepsilon_d + \frac{U}{2} + \frac{1}{4}\left[U + 2\Delta(t,\frac{U}{2})\right]$	1
$\|2,0,0\rangle_o = \frac{1}{\sqrt{2}}\left[\|2,0,0\rangle_1 - \|2,0,0\rangle_2\right]$	$2\varepsilon_d + U$	1
$\|2,1,m\rangle_o = \|2,1,m\rangle$	$2\varepsilon_d + \frac{U}{2}$	3
$\|2,0,0\rangle_- = a_2\|2,0,0\rangle_0 + \frac{a_1}{\sqrt{2}}\left[\|2,0,0\rangle_1 + \|2,0,0\rangle_2\right]$	$2\varepsilon_d + \frac{U}{2} + \frac{1}{4}\left[U - 2\Delta(t,\frac{U}{2})\right]$	1

where

$$a_1^2 = \frac{1}{\Delta(t,\frac{U}{2})}\frac{\Delta(t,\frac{U}{2})-\frac{U}{2}}{2} \qquad\qquad a_2^2 = \frac{4t^2}{\Delta(t,\frac{U}{2})}\frac{2}{(\Delta(t,\frac{U}{2})-\frac{U}{2})}$$

These states have the same form as in the case of the Hubbard dimer, but the ground state energy and the values of a_1 and a_2 are different. Finally, for $N = 3$ electrons, the eigenstates are

$\|3,S,S_z\rangle_\alpha$	$E_\alpha(3,S)$	$d_\alpha(3,S)$
$\|3,1/2,\sigma\rangle_+ = \alpha_2\|1,1/2,\sigma\rangle_1 + \alpha_1\|1,1/2,\sigma\rangle_2$	$3\varepsilon_d + U + \frac{1}{4}[U + \Delta(t,U)]$	2
$\|3,1/2,\sigma\rangle_- = \alpha_1\|1,1/2,\sigma\rangle_1 - \alpha_2\|1,1/2,\sigma\rangle_2$	$3\varepsilon_d + U + \frac{1}{4}[U - \Delta(t,U)]$	2

References

[1] K.F. Sundman, Acta Mathematica **36**, 105 (1912)

[2] F. Diacu, *The Mathematical Intellingencer* **18**, 66 (1996)

[3] Y.N. Harari, *Homo Deus: A Brief History of Tomorrow*,
Harvill Secker, Penguin Random House UK (2016)

[4] W. Metzner and D. Vollhardt, Phys. Rev. Lett. **62**, 324 (1989)

[5] E. Müller-Hartmann, Z. Phys. B **74**, 507 (1989);
Z. Phys. B **76**, 211 (1989); Int. J. Mod. Phys. B **3**, 2169 (1989)

[6] A. Georges and G. Kotliar, Phys. Rev. B **45**, 6479 (1992)

[7] M. Jarrell, Phys. Rev. Lett. **69**, 168 (1992)

[8] E. Pavarini, E. Koch, R. Scalettar, R. Martin (Eds):
The Physics of Correlated Insulators, Metals, and Superconductors,
Reihe Modeling and Simulation, Vol. 7 (Forschungszentrum Jülich, 2017)
`http://www.cond-mat.de/events/correl17`

[9] E. Koch, G. Sangiovanni, and O. Gunnarsson, Phys. Rev. B **78**, 115102 (2008)

[10] A. Flesch, E. Gorelov, E. Koch, E. Pavarini, Phys. Rev. B **87**, 195141 (2013)

[11] A. Kiani and E. Pavarini, Phys. Rev. B **94**, 075112 (2016)

[12] E. Pavarini, E. Koch, A. Lichtenstein, D. Vollhardt (Eds.):
The LDA+DMFT approach to strongly-correlated materials,
Reihe Modeling and Simulation, Vol. 1 (Forschungszentrum Jülich, 2011)
`http://www.cond-mat.de/events/correl11`

[13] E. Pavarini, E. Koch, A. Lichtenstein, D. Vollhardt (Eds.):
DMFT at 25: Infinite Dimensions,
Reihe Modeling and Simulation, Vol. 4 (Forschungszentrum Jülich, 2014)
`http://www.cond-mat.de/events/correl14`

[14] E. Pavarini, A. Yamasaki, J. Nuss, and O.K. Andersen,
New. J. Phys **7**, 188 (2005)

[15] N. Marzari, A.A. Mostofi, J.R. Yates, I. Souza, and D. Vanderbilt,
Rev. Mod. Phys. **84**, 1419 (2012)

[16] G. Zhang and E. Pavarini, Phys. Status Solidi RRL, 1800211 (2018)

[17] E. Pavarini, S. Biermann, A. Poteryaev, A.I. Lichtenstein, A. Georges, and O.K. Andersen, Phys. Rev. Lett. **92**, 176403 (2004)

[18] O. Gunnarsson, E. Koch, and R.M. Martin, Phys. Rev. B **56**, 1146 (1996)

[19] E. Koch, O. Gunnarsson, and R.M. Martin, Phys. Rev. B **60**, 15714 (1999)

[20] See L. de' Medici, *Hund's Metals Explained*, in Ref. [8]

[21] G. Zhang, E. Gorelov, E. Sarvestani, and E. Pavarini, Phys. Rev. Lett. **116**, 106402 (2016)

[22] A. Damascelli, D.H. Lu, K.M. Shen, N.P. Armitage, F. Ronning, D.L. Feng, C. Kim, Z.-X. Shen, T. Kimura, Y. Tokura, Z.Q. Mao, and Y. Maeno, Phys. Rev. Lett. **85**, 5194 (2000)

[23] E. Sarvestani, G. Zhang, E. Gorelov, and E. Pavarini, Phys. Rev. B **97**, 085141 (2018)